

1 **Non-OH chemistry in oxidation flow reactors for the study of atmospheric chemistry**
2 **systematically examined by modeling**

3 Z. Peng^{1,2}, D.A. Day^{1,2}, A.M. Ortega^{1,3,*}, B.B. Palm^{1,2}, W.W. Hu^{1,2}, H. Stark^{1,2,5}, R. Li^{1,3,4,**}, K. Tsigaridis⁶, W.H. Brune⁷,
4 and J.L. Jimenez^{1,2}

5 ¹ Cooperative Institute for Research in Environmental Sciences, University of Colorado, Boulder, CO 80309, USA

6 ² Department of Chemistry and Biochemistry, University of Colorado, Boulder, CO 80309, USA

7 ³ Department of Atmospheric and Oceanic Sciences, University of Colorado, Boulder, CO 80309, USA

8 ⁴ Chemical Sciences Division, Earth System Research Laboratory, National Oceanic and Atmospheric
9 Administration, Boulder, CO 80305, USA

10 ⁵ Aerodyne Research, Inc., Billerica, MA 01821, USA

11 ⁶ Center for Climate Systems Research, Columbia University, and NASA Goddard Institute for Space Studies, New
12 York, NY 10025, USA

13 ⁷ Department of Meteorology, Pennsylvania State University, University Park, PA 16802, USA

14 * now at: Chemical and Environmental Engineering, University of Arizona, Tucson, AZ 85721, USA

15 ** now at: Markes International, Inc., Cincinnati, OH 45242, USA

16 Correspondence to: J.L. Jimenez (jose.jimenez@colorado.edu)

17

18 **Abstract.** Oxidation flow reactors (OFRs) using low-pressure Hg lamp emission at 185 and 254 nm
19 produce OH radicals efficiently and are widely used in atmospheric chemistry and other fields. However,
20 knowledge of detailed OFR chemistry is limited, allowing speculation in the literature about whether
21 some non-OH reactants, including several not relevant for tropospheric chemistry, may play an
22 important role in these OFRs. These non-OH reactants are UV radiation, O(¹D), O(³P), and O₃. In this
23 study, we investigate the relative importance of other reactants to OH for the fate of reactant species in
24 OFR under a wide range of conditions via box modeling. The relative importance of non-OH species is
25 less sensitive to UV light intensity than to water vapor mixing ratio (H₂O) and external OH reactivity
26 (OHR_{ext}), as both non-OH reactants and OH scale roughly proportionally to UV intensity. We show that
27 for field studies in forested regions and also the urban area of Los Angeles, reactants of atmospheric
28 interest are predominantly consumed by OH. We find that O(¹D), O(³P), and O₃ have relative
29 contributions to VOC consumption that are similar or lower than in the troposphere. The impact of O
30 atoms can be neglected under most conditions in both OFR and troposphere. We define “riskier OFR
31 conditions” as those with either low H₂O (<0.1%) or high OHR_{ext} (≥100 s⁻¹ in OFR185 and >200 s⁻¹ in
32 OFR254). We strongly suggest avoiding such conditions as the importance of non-OH reactants can be
33 substantial for the most sensitive species, although depending on the species present OH may still
34 dominate under some riskier conditions. Photolysis at non-tropospheric wavelengths (185 and 254 nm)
35 may play a significant (>20%) role in the degradation of some aromatics, as well as some oxidation
36 intermediates, under riskier reactor conditions, if the quantum yields are high. Under riskier conditions,
37 some biogenics can have substantial destructions by O₃, similarly to the troposphere. Working under
38 low O₂ (volume mixing ratio of 0.002) with the OFR185 mode allows OH to completely dominate over
39 O₃ reactions even for the biogenic species most reactive with O₃. Non-tropospheric VOC photolysis may
40 have been a problem in some laboratory and source studies, but can be avoided or lessened in future
41 studies by diluting source emissions and working at lower precursor concentrations in laboratory studies,
42 and by humidification. Photolysis of SOA samples is estimated to be significant (>20%) under the upper
43 limit assumption of unity quantum yield at medium (1x10¹³ and 1.5x10¹⁵ photons cm⁻² s⁻¹ at 185 and
44 254 nm, respectively) or higher UV flux settings. The need for quantum yield measurements of both
45 VOC and SOA photolysis is highlighted in this study. The results of this study allow improved OFR
46 operation and experimental design, and also inform the design of future reactors.

47 1 Introduction

48 For decades, environmental chambers have been employed to study atmospheric chemical processes,
49 particularly, volatile organic compound (VOC) oxidation processes in the atmosphere (Cocker et al., 2001;
50 Carter et al., 2005; Presto et al., 2005; Wang et al., 2011; Platt et al., 2013), without the interference of
51 some transport processes (e.g., advection and wet deposition). These oxidation processes are the key
52 to secondary organic aerosol (SOA) formation (Odum et al., 1996; Hoffmann et al., 1997; Hallquist et al.,
53 2009), and air pollutant removal (Levy II, 1971). Atmospheric simulation chambers usually have volumes
54 on the order of several m³, and use light sources longer than 300 nm (e.g., sunlight or UV blacklights) to
55 generate oxidants (mainly OH). These settings leads to OH concentrations (10⁶–10⁸ molecules cm⁻³) that
56 are not much higher than the typical ambient values (10⁶–10⁷ molecules cm⁻³; Mao et al., 2009).
57 Relatively low OH concentrations require long residence/simulation times (generally hours) and limit
58 the ability of those setups to reach very high photochemical ages that are atmospherically-relevant
59 (George et al., 2007; Kang et al., 2007; Carlton et al., 2009; Seakins, 2010; Wang et al., 2011). Residence
60 times are ultimately limited due to losses of gases and particles to Teflon walls with timescales of tens
61 of minutes to several hours (Cocker et al., 2001; Matsunaga and Ziemann, 2010; Zhang et al., 2014) as
62 well as by the limited volume of the bag relative to the sampling instrumentation (Nguyen et al., 2014).
63 Besides, large sizes and support systems (e.g. clean air generators) make it difficult to use large
64 chambers in field or source studies.

65 Oxidation flow reactors (OFR) are an alternative that offers some advantages over environmental
66 chambers, especially for rapid changes of experimental conditions, and/or for field experiments. They
67 generally have a smaller size (on the order of 10 L), and typically use low-pressure Hg lamps as light
68 sources for producing OH in large amounts via O₃ and/or H₂O photolysis. These design choices lead to
69 good portability, short experimental timescales, ability to reach long photochemical ages, and
70 potentially reduced wall losses.

71 Due to these advantages, OFRs have been employed in many recent field and laboratory studies
72 in atmospheric chemistry, particularly in SOA-related research (George et al., 2007; Kang et al., 2007,
73 2011; Smith et al., 2009; Massoli et al., 2010; Cubison et al., 2011; Lambe et al., 2011a, 2011b, 2012,
74 2013; Bahreini et al., 2012; Saukko et al., 2012; Wang et al., 2012; Ortega et al., 2013; Li et al., 2013).
75 OFRs are also used in related applied fields, such as scrubbing of pollution from air (Johnson et al., 2014).
76 In contrast to their popularity, the chemistry occurring in OFRs is still incompletely characterized,
77 although the formation and interconversion reactions of most oxidants in OFRs have been well
78 characterized (Sander et al., 2011; Ammann et al., 2015). To our knowledge, there are only three studies
79 of OFR radical oxidation chemistry up to date: Ono et al. (2014) focused on the dependence of O₃
80 destruction on H₂O concentration. We have recently made progress on the characterization of HO_x
81 radical chemistry in OFRs (Li et al., 2015; Peng et al., 2015). We have developed a kinetic model for OFRs,
82 which provides predictions in good agreement with laboratory experiments. This model has also shown
83 that OH exposure (OH_{exp}, i.e., OH concentration integrated over the reactor residence time) increases
84 with H₂O concentration and UV intensity, and decreases with external OH reactivity [OHR_{ext} = ∑k_iC_i, i.e.,

85 the sum of the products of concentrations of externally introduced OH-consuming species (c_i) and rate
86 constants of their reactions with OH (k_i]. The OH_{exp} decrease due to OHR_{ext} was defined as “OH
87 suppression,” and can reach two orders-of-magnitude in some cases (Li et al., 2015; Peng et al., 2015).
88 We also showed that relative uncertainties of the outputs of our box model (e.g., OH_{exp}) due to uncertain
89 kinetic parameters are typically only 20% (Peng et al., 2015). However, none of these studies directly
90 address the fate of VOCs (including oxygenated VOCs), simply regarded as external OH reactants in the
91 prior studies.

92 The primary reason for the use of the OFRs studied here is for the study of reactions of species or
93 mixtures of atmospheric relevance with the OH radical. However, other highly reactive species are also
94 present at very elevated concentrations, including the radicals $\text{O}(^1\text{D})$ and $\text{O}(^3\text{P})$, 185 and 254 nm photons,
95 and O_3 . If a substantial fraction of the species of interest reacted with those non-OH reactants, then the
96 chemistry in the OFR would deviate from the OH radical chemistry intended to investigate. The absence
97 of systematic research on VOC fate in OFRs leaves room for some speculation that non-OH or non-
98 tropospheric chemistry can play a major role in OFRs: for example, Johnson et al. (2014) suggested that
99 $\text{O}(^1\text{D})$ and $\text{O}(^3\text{P})$ significantly consumed VOCs. Klems et al. (2015) concluded that photons at 254nm
100 from Hg-lamp emission played an important role in their OFR experiment, especially for downstream
101 chemistry. Lack of clarity about these types of questions and of clear guidelines about how to apply
102 OFRs to avoid such problems have limited the application of OFRs for years. In this paper, we apply the
103 model in Peng et al. (2015) to systematically investigate whether significant non-tropospheric or non-
104 OH chemistry occurs in OFRs, and what experimental conditions make it more important. Considering
105 the enormous complexity of organic radical (particularly organic peroxy) chemistry, we only examine
106 the non-OH fate of stable species in the present work. The fate of organic radicals should be the subject
107 of future studies. The results allow improved OFR operation and experimental design, as well as
108 guidance for the design of future reactors.

109 **2 Methods**

110 The OFR and the model used here have been described in detail elsewhere (Kang et al., 2007; Li et
111 al., 2015; Peng et al., 2015). Here, we only present a brief introduction for each.

112 **2.1 Potential Aerosol Mass flow reactor**

113 Kang et al. (2007) first introduced the Potential Aerosol Mass (PAM) flow reactor. Although there
114 were earlier versions of the PAM reactor, the version of cylindrical geometry with a volume of ~13 L has
115 been widely used and is currently in use in many SOA research groups (Massoli et al., 2010; Cubison et
116 al., 2011; Kang et al., 2011; Lambe et al., 2011a, 2011b, 2012, 2013; Bahreini et al., 2012; Saukko et al.,
117 2012; Wang et al., 2012; Li et al., 2013; Ortega et al., 2013). The reactor is made of aluminum or of glass
118 and aluminum, and equipped with 1–4 low-pressure Hg lamps (model no. 82-9304-03, BHK Inc.) located
119 inside the flow tube. The Hg lamps produce UV emissions at 185 and 254 nm, whose intensity can be
120 rapidly computer-controlled. The operation mode using both 185 and 254 nm emissions is called
121 “OFR185”. In this mode, photons at 185 nm dissociate H_2O and O_2 molecules to produce $\text{OH}+\text{H}$ and

122 O(³P), respectively. Recombination of O(³P) with O₂ forms O₃. UV light at 254 nm then photolyzes O₃ to
123 produce O(¹D), which reacts with H₂O and produces additional OH. OFR can also be operated in another
124 mode where photons at 185 nm are filtered by quartz sleeves around the lamps. In this case, only 254
125 nm UV light is active to generate OH (“OFR254” mode), and injection of externally generated O₃ into
126 the reactor is required for OH production. The amount of injected O₃ plays a critical role in the OFR
127 chemistry (Peng et al., 2015). For this reason this amount (X ppm) is also included in OFR operation
128 mode notation in the form of OFR254-X. For example, OFR254-70 and OFR254-7 denote experiments
129 with 70 and 7 ppm O₃ injected, respectively. We use the PAM as the basic OFR design. Other designs
130 will be specified below if needed. Rapid computer-controlled UV lamp setting allows rapidly scanning
131 UV lamp settings during an experiment, and has unique applications to OFR experiments in field studies
132 (Hu et al., 2015; Ortega et al., 2015; Palm et al., 2015). In these experiments, OFRs enable the
133 exploration of a very large range of photochemical age during a short period (~2 hr) when ambient
134 conditions often do not significantly change.

135 **2.2 Model description**

136 We use the same model as in Peng et al. (2015), a standard chemical-kinetic model under plug-
137 flow conditions. The effect of non-plug flow residence time distributions (RTD) was also investigated in
138 that study. Non-plug-flow models result in similar OH_{exp} than plug-flow in most cases, except under
139 specific conditions with very high UV, H₂O, and OHR_{ext} (Peng et al., 2015). Therefore, plug-flow OH_{exp} is
140 used in this study, as a proxy of OH_{exp} estimated from OHR_{ext} decay and to avoid the much increased
141 computational expense for complex RTDs. All O_x and HO_x reactions available in the JPL Chemical Kinetic
142 Data Evaluation (Sander et al., 2011) are taken into account. Reactions of some external OH reactants
143 (externally introduced reactants destructing OH), such as SO₂, CO and NO_x, are also included. SO₂ is used
144 as a proxy of other external OH reactants (e.g., VOCs). We believe that this is a realistic approximation
145 in terms of OHR_{ext} decay vs. OH_{exp} for many precursors, as discussed in Peng et al. (2015).

146 When studying the OFR, we assume a residence time of 180 s, and use typical temperature (295
147 K) and atmospheric pressure (835 mbar) in Boulder, CO, USA. H₂O mixing ratio (abbr. H₂O hereafter)
148 ranges from 0.07 to 2.3% (equivalent to relative humidity (RH) of 3–92%). According to Li et al. (2015),
149 UV photon fluxes (abbr. UV hereafter) at 185 and 254 nm are estimated to be in the ranges 1.0x10¹¹–
150 1.0x10¹⁴ and 4.2x10¹³–8.5x10¹⁵ photons cm⁻² s⁻¹, respectively. Four levels of OHR_{ext}, 0, 10, 100, and 1000
151 s⁻¹ covering the range of most field and laboratory studies are investigated. In the explored parameter
152 space, the same 3-character labels as in Peng et al. (2015) are used to denote typical cases (Table 1). For
153 OFR254, we study OFR254-70 and OFR254-7, representing OFR254 experiments with high (Palm et al.,
154 2015) and low O₃ (Kang et al., 2011; Liu et al., 2015), respectively. To model literature OFR studies, we
155 adopt corresponding parameters (reactor volume, H₂O, residence time, etc.), and estimate parameters
156 that are specified or measured (e.g., UV) as needed. In particular, for some field studies, where long
157 time-series of experimental data [42 d in BEACHON-RoMBAS (Palm et al., 2015), 42 d in SOAS (Hu et al.,
158 2015), and 15 d in CalNex-LA (Ortega et al., 2015)] were recorded, we model all valid datapoints and
159 present outputs in the form of histograms. Note that the outputs for field studies, i.e., histograms, have

160 a complex dependence on ambient temperature, H₂O, and OHR_{ext}, as well as UV steps used. The specific
161 histogram shapes for different field campaigns are influenced by both ambient and experimental
162 parameters.

163 **3 Results and Discussions**

164 In the following sections we explore the relative importance of five non-OH pathways (photons at
165 185 and 254 nm, O(¹D), O(³P), and O₃) vs. the OH reaction for species of atmospheric interest, including
166 a variety of typical biogenic and anthropogenic VOCs and a few important inorganic species (e.g., SO₂
167 and NO₂). Because of the huge complexity of VOC oxidation mechanisms, only consumption/oxidation
168 of specific VOCs is investigated. In such an investigation, a large amount of kinetic data is required. We
169 collected the required data (Tables S1–S3) according to the principles in Section S1. Photolysis of SOA is
170 also investigated.

171 **3.1 Fractional loss of VOCs to non-OH reactants**

172 As shown in Peng et al. (2015), OH_{exp} in OFRs depends on various physical conditions, e.g., H₂O and
173 OHR_{ext}. However, the non-OH reactants are much less dependent on these parameters. H₂O and
174 external OH reactants only contribute less than 1% to absorption at 185 and 254 nm. Therefore, they
175 have almost no impact on effective UV. O₃ can absorb a fraction of the 254 nm radiation, but the optical
176 depth due to 70 ppm O₃ in the reactor is ~0.11, and thus the attenuation of 254 nm photons by O₃
177 absorption is a minor effect. The dominant fates of O(¹D) and O(³P) are the quenching by air and the
178 recombination with O₂, respectively, with which no reactions involving H₂O or external OH reactants can
179 compete. Thus the concentrations of O(¹D) and O(³P) in the reactor depend on UV intensity and H₂O,
180 but not on OHR_{ext}. Since OH can be strongly modulated by OHR_{ext}, changing input conditions may result
181 in very different relative importance of OH to other reactive species. To fully evaluate this issue, it is
182 necessary to explore a very wide range of conditions as in Peng et al. (2015).

183 **3.1.1 Common features of all the non-OH reactants**

184 Figs. 1–5 show the relative consumption of several species vs. ratio of exposures to individual non-
185 OH species (X) to OH exposure ($X_{\text{exp}}/\text{OH}_{\text{exp}}$) for 185 and 254 nm photons, O(¹D), O(³P), and O₃,
186 respectively. Fig. S1-S5 present the same information in an alternative format that may be useful to
187 evaluate the fate of species not included in our study. They show ratios of rate constants of species with
188 OH to those with non-OH species (X), mathematically equivalent to the $X_{\text{exp}}/\text{OH}_{\text{exp}}$ where corresponding
189 $X/(\text{OH}+X)$ is 50%. $X/(\text{OH}+X)$ denotes the fractional importance of X in the sum of the contribution of OH
190 and X to VOC. If a VOC has a higher ratio of rate constant with OH to that with a non-OH reactant (X)
191 than with another reactant (Y), the relative contribution of X, $X/(\text{OH}+X)$, should be smaller than that of
192 Y. In these figures, we also show the $X_{\text{exp}}/\text{OH}_{\text{exp}}$ range for OFR254-70, OFR254-7, and OFR185, under
193 different conditions, including key laboratory and field studies, and identify the $X_{\text{exp}}/\text{OH}_{\text{exp}}$ ranges where
194 non-OH contribution to species fate is significant. A dissociation quantum yield of unity is assumed for
195 the photolysis reactions, which results in upper limits for the relative importance of those pathways.

196 In these figures, the relationships of all non-OH reactive species to OH are similar for certain
197 common conditions. We define three types of conditions to help guide experimental design and

198 evaluation in terms of the relative importance of non-OH reactants. Under “riskier conditions” of
199 high/very high $\text{OHR}_{\text{ext}} (\geq 100 \text{ s}^{-1}$ in OFR185 and $>200 \text{ s}^{-1}$ in OFR254 (-7 to -70)) and/or low H_2O ($<0.1\%$),
200 non-OH reactions can be significant depending on the species. Conversely, under “safer conditions” with
201 relatively low $\text{OHR}_{\text{ext}} (<30 \text{ s}^{-1}$ in OFR185 and $<50 \text{ s}^{-1}$ in OFR254), and high H_2O ($>0.8\%$ in OFR185 and $>0.5\%$
202 in OFR254), and moderate or higher UV ($>1 \times 10^{12}$ photons $\text{cm}^{-2} \text{ s}^{-1}$ at 185 nm) in OFR185, reaction with
203 OH is dominant (Figs. 1–5 and S1–5). We denote all other conditions as “transition conditions.” High
204 H_2O and zero/low OHR_{ext} lead to strong OH production and no/weak OH suppression, respectively. Thus,
205 OH is more abundant and dominates species consumption under those conditions. In the case of low
206 H_2O and high OHR_{ext} , OH is generally lower because of less production and more suppression. These
207 conditions increase the relative contribution of non-OH species. UV light intensity is generally less
208 influential on non-OH VOC fate than H_2O and OHR_{ext} , although OH production is nearly proportional to
209 UV (Peng et al., 2015), because the non-OH reactive species also scale (nearly) proportional to UV. As a
210 result, UV generally has smaller effects on exposure ratios between OH and the non-OH reactants.
211 However, under a UV near the lower bound of the explored range in this study ($<1 \times 10^{12}$ photons $\text{cm}^{-2} \text{ s}^{-1}$
212 at 185 nm) in OFR185, OH production is so small that the effect of OHR_{ext} on OH suppression can be
213 amplified and hence some exposure ratios may be affected. In OFR254 OH is more resilient to
214 suppression even at low UV because of the OH-recycling by initially injected O_3 (Peng et al., 2015). Note
215 that we call these conditions “riskier” and “safer” mainly in terms of non-tropospheric VOC fate, but
216 not of VOC fate by all non-OH reactants, as some of the non-OH reactant studied in this work may also
217 play a role under some tropospheric conditions (see Sections 3.1.4 and 3.1.5). In addition to the
218 common features above, individual non-OH reactants have their own features as well as a few
219 exceptions to the above mentioned general observations, which we will detail below.

220 **3.1.2 Reactions with OH vs. photolysis at 185 nm**

221 Under riskier reactor conditions, photolysis at 185 nm of several aromatic compounds, such as
222 toluene, benzene, and p-xylene, are estimated to be significant and even dominant vs. the OH reactions
223 (Fig. 1). This results from their aromatic ring, which is not only highly efficient as a chromophore, but
224 also relatively resistant to OH attack.

225 It is not common to perform field studies for SOA at H_2O as low as 0.1% or $\text{OHR}_{\text{ext}} \geq 100 \text{ s}^{-1}$ (Table
226 1). According to $F_{185\text{exp}}/\text{OH}_{\text{exp}}$ calculated from the field studies where OFR185 was deployed, i.e.,
227 BEACHON-RoMBAS (Palm et al., 2015), SOAS (Hu et al., 2015), and CalNex-LA (Ortega et al., 2015) all
228 these studies are generally under safer conditions (infrequent low H_2O mixing ratio and ambient OH
229 reactivity estimated to be $\sim 15\text{--}25 \text{ s}^{-1}$). For instance, none of these field studies fell into the conditions
230 where the fractional importance of photolysis at 185 nm was significant for aromatic species. However,
231 in some source studies using OFRs, e.g. when sampling biomass burning smoke (FLAME-3; Ortega et al.
232 2013) or air in a traffic tunnel (Tkacik et al., 2014), OHR_{ext} can be very high reaching values of several
233 100 s^{-1} (Table S4). Especially on the smoke study, photolysis of aromatics may have played a role.
234 However, it has long been known that excited aromatic molecules may undergo various deactivation
235 pathways (e.g., vibronic coupling, intersystem crossing, and collisional quenching) without molecular

236 fragmentation (Beddard et al., 1974; Nakashima, 1982; Nakashima and Yoshihara, 1983; Fang and
237 Phillips, 2002), preventing unity quantum yields. Therefore, the photolysis of aromatics at 185 nm in the
238 above mentioned source studies may not be as significant as estimated in Fig. 1.

239 Under riskier conditions, some organic peroxy nitrates and nitrates (e.g., peroxyacetyl nitrate and
240 2-propyl nitrate in Fig. 1) have an estimated contribution from photolysis at 185 nm to their fate that is
241 comparable to or even larger than that of reaction with OH. Nevertheless, this does not mean that we
242 need to make extra efforts to avoid the photolysis of organic nitrates and peroxy nitrates at 185 nm.
243 Although they have cross-sections at 185 nm ~10–100 times smaller than those of aromatics, these
244 organic compounds react remarkably slowly with OH (~2 order of magnitude slower than reactions of
245 aromatics with OH), so photolysis appears substantial with respect to reaction with OH, but really two
246 slow rates are being compared. Thus, absolute photolyzed amounts of these species are not substantial.
247 For example, only ~10% of peroxyacyl nitrate is photolyzed by 185 nm photons at the highest OFR185
248 lamp setting. Even if photolysis of nitrates and peroxy nitrates by low-pressure Hg lamp emission
249 proceeds to a significant extent, it may still not be a problem, as it generally leads to the same products
250 as their ambient photolysis (Renlund and Trott, 1984; Roberts and Fajer, 1989). Nitrate and peroxy
251 nitrate photolysis is actually much more important in the atmosphere than in OFRs for the same
252 photochemical age (see below and Fig. 6).

253 SO₂ has been used in some studies to calibrate OH_{exp} (Lambe et al., 2015; Li et al., 2015). It does
254 undergo significant photolysis at 185 nm under riskier conditions. However, this photolysis does not
255 lead to an overestimation of OH_{exp}, since the S-bearing product of SO₂ photolysis at 185 nm, SO, converts
256 back to SO₂ very rapidly through its reaction with O₂.

257 Oxidation intermediates may also photolyze at 185 nm. However, their photolysis is unlikely to be
258 significant when OFR is operated under safer conditions. To clarify this issue, a detailed discussion about
259 the photolysis of oxidation intermediates at 254 nm is required as a premise. We thus discuss oxidation
260 intermediate photolysis at both 185 and 254 nm in Section 3.1.3.

261 **3.1.3 Reactions with OH vs. photolysis at 254 nm**

262 The photon flux in the reactor at 254 nm is 80–250 times larger than at 185 nm (Li et al., 2015).
263 Although absorption cross sections of all molecules investigated in this study are significantly lower at
264 254 than 185 nm, the higher photon flux compensates, at least partially, for this effect, so that in OFR185
265 photolysis of many species at 254 nm is of similar relative importance as photolysis at 185 nm, with
266 potentially important effects at low H₂O and/or high OHR_{ext} (Figs. 2 and S2). As for 185 nm, 254 nm
267 photolysis is a concern mainly for aromatic compounds, because of the high light absorptivity and low
268 OH reactivity of aromatic rings as previously discussed. Again, note that this concern may be less serious
269 than shown in Fig. 2 because of possible lower quantum yields. Photolysis of organic nitrates and peroxy
270 nitrates at 254 nm also appears to be important relative to reactions with OH, and is still not a concern
271 for the same reasons as photolysis at 185 nm. SO₂ can absorb efficiently at 254 nm, but it is still not a
272 problem for SO₂-based OH_{exp} calibration, since photons at 254 nm are not sufficiently energetic to
273 dissociate SO₂ molecules.

274 High UV generally appears to be more problematic than low UV in OFR254 (Fig. S2). This is in
275 contrast to the trend of OFR185. In OFR254, O₃ is the only primary OH source, and a substantial fraction
276 of O₃ can be photolyzed at the highest lamp settings, leading to a substantial reduction of OH production
277 (compared with proportional scaling with UV). OFR254-70 appears to be less prone to riskier conditions
278 than OFR254-7, since higher O₃ favors HO₂-to-OH recycling, making OH more resilient to suppression
279 (Peng et al., 2015).

280 Under highly risky conditions (H₂O<0.1% and OHR_{ext}≥100 s⁻¹ for OFR185, and H₂O<0.1% and
281 OHR_{ext}>200 s⁻¹ for OFR254), some saturated carbonyl compounds (e.g., pyruvic acid, methyl ethyl ketone
282 and hydroxyacetone) have significant photolysis at 254 nm relative to reactions with OH. This significant
283 relative contribution of photolysis also results from remarkably slow reactions of saturated carbonyl
284 compounds with OH. Although secondary species without C=C double bond, e.g., saturated carbonyls,
285 hydroperoxides, and nitrates, can be photolyzed in OFRs at low H₂O and/or high OHR_{ext}, their photolysis
286 only proceeds to a ~10–1000 times smaller extent than ambient photolysis at the same photochemical
287 age (Fig. 6).

288 Unsaturated carbonyls may have much higher absorption cross-sections if their C=C bonds are
289 conjugated with carbonyls. However, according to our following analysis, conjugated unsaturated
290 carbonyl compounds do not often cause problems of non-tropospheric photolysis at 254 nm. Carbonyls
291 have π–π* and n–π* transitions. The former corresponds to high cross-section (typically >10⁻¹⁸ cm²) and
292 typically occurs around or below 200 nm. The latter is forbidden, and thus has weak absorption (cross-
293 section on the order of 10⁻¹⁹ cm² or lower), and typically occurs around or above 300 nm (Turro et al.,
294 2009). Conjugation usually does not substantially enhance the absorption of n–π* transition but it does
295 for π–π* transitions (Turro et al., 2009). As a result, through conjugation, the only reason why cross-
296 sections of carbonyls at 254 nm may be elevated above 10⁻¹⁸ cm² is the red-shift of the maximum
297 absorption wavelength of their π–π* transitions due to conjugation. According to Woodward's rules
298 (Pretsch et al., 2009) and available cross-section data of α,β-unsaturated carbonyls in Keller-Rudek et al.
299 (2015), a conjugation of at least 3–4 double bonds is required for the excitation at 254 nm to dominantly
300 correspond to π–π* transition. Conjugated oxidation intermediates containing at least 3–4 double
301 bonds including C=C bond(s) are virtually impossible to form from aliphatic hydrocarbon oxidation in
302 OFRs. Nevertheless, such intermediates may form via ring-opening pathways of aromatic oxidation
303 (Calvert et al., 2002; Atkinson and Arey, 2003; Strollo and Ziemann, 2013). E,E-2,4-hexadienedial may
304 be regarded as an example of this type of intermediates. Even under assumption of a unity quantum
305 yield, its fraction of photolysis at 254 nm is not much higher than that of aromatic precursors (Fig. 2).
306 Therefore, 254 nm photolysis of conjugated intermediates should not be problematic as long as safer
307 experimental conditions are adopted.

308 To our knowledge, the only exception that has strong absorption at 254 nm due to conjugation
309 with <2 double bonds are β-diketones, which may be formed in aliphatic hydrocarbon oxidation,
310 particularly that of long-chain alkanes (Ziemann and Atkinson, 2012). The peculiarity of β-diketones is
311 that their enol form may have a highly conjugated ring structure due to very strong resonance (Scheme

312 S1), and hence cross-sections on the order of 10^{-17} cm² at 254 nm (Messaadia et al., 2015). However,
313 even under the assumption of unity quantum yield, the fractional contribution of 254 nm photolysis of
314 acetylacetone (representative of β -diketones) is only slightly larger than for aromatic VOCs (Fig. 2), since
315 its enol form also contains a C=C bond leading to very high reactivity toward OH. Furthermore, we argue
316 that the actual probability that a concrete structural change (in number and type of functional groups,
317 O/C ratio, average C oxidation state etc.) of β -diketones resulting from photoexcitation at 254 nm may
318 be low. As their excitation at 254 nm corresponds to π - π^* transition, their rigid ring structure likely
319 hinders cyclic structural change at the 1st singlet excited state ($S_1(\pi,\pi^*)$) while the biradical structure of
320 the 1st triplet state ($T_1(\pi,\pi^*)$) may favor H-shift between two O atoms, which ends up with the
321 same/similar structure than prior to the H-shift (Scheme S1). Also, the excitation of β -diketones at 254
322 nm may also lead to charge transfer complex formation via direct excitation and/or radiationless
323 transition from a local excited state (Phillips and Smith, 2015), which is likely to result in low quantum
324 yields, as discussed in detail below.

325 In addition to conjugated species, Phillips and Smith (2014, 2015) reported a new type of highly
326 absorbing species that may be formed from VOC oxidation. Although their studies were conducted in
327 the condensed phase, it is likely that the main conclusions of these studies are generally transferable to
328 the gas-phase conditions, since no long-range interactions, which do not exist in normal gases, were
329 involved in these studies. Phillips and Smith (2014, 2015) investigated the photoabsorption
330 enhancement of multifunctional oxygenated species in SOA and found that the high absorptivity of
331 these species can largely be explained by transitions toward the electronic states of charge transfer
332 complex formed between hydroxyl groups (donor) and neighboring carbonyl groups (acceptor). They
333 also pointed out that charge transfer complexes of this kind have a continuum of states whose energy
334 levels range from that of local excited states (radiative transition wavelength <300 nm) to very low levels
335 (radiative transition wavelength >600 nm). The latter are insufficient to cause common photochemical
336 reactions. Relaxation through a continuum of states is usually ultrafast according to Fermi's golden rule
337 (Turro et al., 2009), likely leading to low quantum yields of chemical reactions. The low quantum yields
338 may be seen even from species with only one hydroxyl and one carbonyl: the photolysis of 3-hydroxy-
339 3-methyl-2-butanone and 4-hydroxy-2-butanone at wavelengths down to 270 nm has quantum yields
340 around only 0.1 (Bouzidi et al., 2014, 2015). Although measurements of photolysis quantum yield for
341 multifunctional species are challenging and rare, it is reasonable to expect even lower quantum yields
342 for larger and/or highly substituted (by hydroxyl and carbonyl) species, since larger species have more
343 degrees of freedom for relaxation of excited molecules, and more and/or larger complex sites generally
344 lead to more efficient relaxation through a continuum of states, in accordance with common
345 photophysical sense (Sharpless and Blough, 2014). Therefore, even though species with a number of
346 hydroxyls and carbonyls are formed in VOC oxidation and can absorb >1 order of magnitude more
347 efficiently at 254 nm than mono- and difunctional species, they may still have low effective photolysis
348 rates because of low quantum yields.

349 For this type of species, we estimate an upper limit of the fractional importance of their photolysis

350 at 254 nm. Molar absorption coefficients of charge transfer transitions of organic molecules are usually
351 $\sim 10^3$ – 1×10^4 L mol⁻¹ cm⁻¹, i.e., cross-sections of $\sim 3.9 \times 10^{-18}$ – 3.9×10^{-17} cm² (Foster, 1969). Based on that, it
352 is reasonable to estimate an upper limit of absorption cross-sections of charge transfer transitions of
353 5×10^{-17} cm². On the other hand, photolysis quantum yields of multifunctional species are unlikely to be
354 larger than that of species with only one carbonyl and one hydroxyl, i.e., ~ 0.1 (see discussion above).
355 We thus take 0.1 as an upper limit of photolysis quantum yields. Besides, 6×10^{-12} cm³ molecule⁻¹ s⁻¹ can
356 be a conservative estimate of rate constants of multifunctional oxygenated species with OH, as it is
357 roughly an average value for ketones (Atkinson and Arey, 2003), and the enhancement of H-abstraction
358 by hydroxyl groups (Kwok and Atkinson, 1995; Ziemann and Atkinson, 2012) and the fast abstraction of
359 aldehydic H atoms (Atkinson and Arey, 2003) are completely neglected. With the three estimates
360 combined, the estimated maximum fractional contribution from photolysis at 254 nm to the fate of
361 multifunctional species (Fig. 2) is close to that of E,E-2,4-hexadienedial and acetylacetone.

362 The problem of photolysis of oxidation intermediates at 185 nm is unlikely to be worse than at 254
363 nm. According to available UV spectra of carbonyl compounds in Keller-Rudek et al. (2015), 185 nm is
364 almost always located within the π – π^* transition band, whose maximum cross-section is on the order
365 of 10^{-17} cm². Even if all types of radiative transitions at normal radiation intensity are considered, an
366 approximate upper limit of absorption cross-sections is $\sim 10^{-16}$ cm² (Evans et al., 2013). However, UV
367 intensity at 185 nm in the OFR185 mode is ~ 100 times lower than that at 254 nm (Li et al., 2015). The
368 photolysis rate of oxidation intermediates at 185 nm should thus be generally smaller than at 254 nm.

369 Therefore, in summary, photolysis of oxidation intermediates are, to our knowledge,
370 conservatively estimated to be of limited importance relative to their reactions with OH, as long as the
371 experimental conditions are in the safer range. Although studies on photolysis quantum yields of
372 oxidation intermediates are very sparse, we reason, based on the existing studies on this topic and
373 common photophysical and photochemical rules, that the photolysis quantum yields of these species
374 may be lower than the values assumed in this study (e.g., 1 for E,E-2,4-hexadienedial and acetylacetone
375 and 0.1 for multifunctional species). As a result, actual rates and relative importance of photolysis might
376 be significantly smaller than the upper limits estimated in our study.

377 As discussed for photolysis at 185 nm, in all ambient OFR field studies (BEACHON-RoMBAS, SOAS,
378 and CalNex-LA), reactions with OH dominate over photolysis at 254 nm (Fig. 2). The fractional
379 consumption of several anthropogenic aromatic VOCs, such as benzene and naphthalene, in the urban
380 CalNex-LA campaign by 254 nm photolysis is estimated as a few percent under most conditions and at
381 most $\sim 15\%$. At the BEACHON-RoMBAS and SOAS forested sites, photolysis at 254 nm should be a
382 negligible contributor to the fate of biogenic VOCs such as isoprene and monoterpenes.

383 Some laboratory and source studies may have had an appreciable contribution to aromatic species
384 fate from 254 nm at low H₂O and/or high $\text{OHR}_{\text{ext}} \cdot \text{F}_{254_{\text{exp}}} / \text{OH}_{\text{exp}}$ in the biomass smoke and urban tunnel
385 source studies (source OHR_{ext} up to ~ 300 s⁻¹; Ortega et al., 2013; Tkacik et al., 2014) and the Kang et al.
386 (2011) laboratory study (H₂O down to $\sim 0.1\%$) can be as high as 10^6 – 10^7 cm/s. In this range, photolysis
387 of a few aromatic VOCs (e.g., benzene and naphthalene) at 254 nm could account for ~ 20 – 80% of their

388 destruction.

389 Note that photolysis of oxidation intermediates also needs to be taken into account. If
390 multifunctional species, β -diketones, and extensively conjugated species are photolyzed as shown in Fig.
391 2, these photolyses would be significant in some previous source and laboratory studies examined here,
392 as they were conducted at relatively low H_2O and/or high OHR_{ext} . To our knowledge, none of these
393 studies reported a significant photolysis of oxidation intermediates. Klems et al. (2015) attributed large
394 amounts of fragmentation products detected in their OFR experiments with dodecanoic acid to
395 photolysis of peroxy radicals. However, these products may also be at least partially accounted for by
396 photolysis of carbonyls leading to carbon-chain cleavage via Norrish reactions (Laue and Plagens, 2005).
397 The OFR used by Klems et al. (2015) has a different design from the PAM, which is regarded as the base
398 design in this study. Their reactor employs a light source stronger than the PAM's highest lamp setting,
399 with UV at 254 nm estimated to be $\sim 3 \times 10^{16}$ photons $\text{cm}^{-2} \text{s}^{-1}$ (~ 4 times the value at the highest lamp
400 setting of the PAM OFR) based on the lamp power and the reactor geometry. Such high UV may even
401 result in significant photolysis of saturated carbonyl intermediates, which are very likely formed in the
402 oxidation of long-chain alkane-like dodecanoic acid.

403 **3.1.4 Reactions with OH vs. reactions with $\text{O}(^1\text{D})$ and $\text{O}(^3\text{P})$**

404 The results for these two radicals are shown in Figs. 3–4. The potential impact of $\text{O}(^1\text{D})$ is smaller
405 than for 185 and 254 nm photons, due to the low concentration of $\text{O}(^1\text{D})$ in the reactor. Only for methane
406 may reaction with $\text{O}(^1\text{D})$ be significant, because the reaction of methane with $\text{O}(^1\text{D})$ is close to the
407 collision rate, while CH_4 is the most resistant VOC to H-abstraction by OH. This could be important if CH_4
408 was used for OH_{exp} calibration under riskier reactor conditions, or if the fate of CH_4 is important to the
409 experiment for other reasons. Other VOCs react more slowly with $\text{O}(^1\text{D})$ and much faster with OH. As a
410 result, reactions of VOCs (other than CH_4) with $\text{O}(^1\text{D})$ in all laboratory, field, and source studies
411 previously discussed are almost always negligible. We also note that the ratio of $\text{O}(^1\text{D})_{\text{exp}}/\text{OH}_{\text{exp}}$ in the
412 OFR is actually much lower than in the troposphere (Monks, 2005), except under some riskier conditions.
413 It is believed that the contribution of $\text{O}(^1\text{D})$ to VOC destruction in the atmosphere should be negligible
414 (Calvert et al., 2002), and their relative importance is even lower under most OFR conditions.

415 Reactions with $\text{O}(^3\text{P})$ are small or negligible contributors to VOC consumption except under
416 extreme riskier conditions. Unless at low H_2O ($< 0.1\%$) and very high external OH reactivity ($\sim 1000 \text{s}^{-1}$),
417 VOC consumption by $\text{O}(^3\text{P})$ cannot be larger than 10% of that by OH (Figs. 4 and S4). This results from
418 both very low concentrations of $\text{O}(^3\text{P})$ and relatively low reactivity compared to that of OH. Among the
419 species that we examine, biogenic VOC consumption may have some contribution from $\text{O}(^3\text{P})$ under the
420 abovementioned riskier conditions, due to the higher reactivity of double bonds in these species with
421 $\text{O}(^3\text{P})$. For example α -pinene in the mixture experiments in Kang et al. (2011) may have had a $\sim 5\%$
422 contribution from $\text{O}(^3\text{P})$. Similarly to $\text{O}(^1\text{D})$, $\text{O}(^3\text{P})_{\text{exp}}/\text{OH}_{\text{exp}}$ in the troposphere (Calvert et al., 2002) is
423 higher than in the OFR except for riskier conditions. Thus the relative importance of both $\text{O}(^1\text{D})$ and $\text{O}(^3\text{P})$
424 to OFR chemistry is typically lower than in the troposphere.

425 **3.1.5 Reactions with OH vs. reactions with O_3**

426 Reaction with O₃ is a major, even dominant pathway of the consumption of many biogenic VOCs
427 in the troposphere. However, it is of interest to quantify the relative importance of OH vs. O₃ across OFR
428 experiments (Figs. 5 and S5). This allows comparison with the relative importance in the troposphere,
429 as well as potentially designing experiments where the relative influence of O₃ is minimized or adjusted
430 as desired.

431 A large amount of O₃ is injected into OFR254, and O₃ concentration in that type of reactor does
432 not change much with UV flux (negligibly under most conditions and up to a factor of ~2 at high H₂O
433 and UV, Peng et al. 2015). Since OH_{exp} is proportional to UV flux, as UV decreases, OH_{exp} is lowered and
434 the fractional species destruction by O₃ increases. In OFR185, O₃ production is almost linearly
435 dependent on UV, while a significant portion of OH production has a quadratic relationship with UV.
436 Thus OH increases faster with increasing UV than O₃. Therefore, lower UV in OFR185 also leads to a
437 higher relative importance of O₃ for VOC consumption.

438 The distribution of O_{3exp}/OH_{exp} expected for the troposphere was obtained from the GISS ModelE2
439 climate model (Schmidt et al., 2014) and is estimated as the ratio of the simulated daily mean
440 concentration of O₃ and OH on a horizontal grid of 2 degrees in latitude and 2.5 degrees in longitude for
441 the year 2000. Interestingly, the simulated relative importance of O₃ to OH in the troposphere is higher
442 than when OFRs are operated under safer conditions, and similar to OFRs when they are operated under
443 riskier conditions (Figs. 5 and S5). In those cases, a number of biogenic VOCs can be significantly
444 consumed by O₃. In particular, some monoterpenes (e.g., α-terpinene) and sesquiterpenes (e.g., β-
445 caryophyllene) have a fractional reaction with O₃ close to 100% in the troposphere. In contrast to
446 biogenics, reactions with O₃ do not play any role in the consumption of most anthropogenic VOCs, e.g.,
447 benzene, toluene, and alkanes. Besides, ozonolysis of saturated oxidation intermediates (e.g. carbonyls
448 and alcohols) is minor or negligible in both OFRs and the atmosphere, since they react with OH at ~10⁻¹³-
449 10⁻¹¹ cm³ molecule⁻¹ s⁻¹ while their ozonolysis rate constants are <10⁻²⁰ cm³ molecule⁻¹ s⁻¹ (Atkinson
450 and Arey, 2003). However, unsaturated oxidation intermediates may have larger contributions from O₃
451 because of C=C bonds. In particular, dihydrofurans, possible intermediates of saturated hydrocarbon
452 oxidation (Ziemann and Atkinson, 2012; Aimanant and Ziemann, 2013), may be predominantly oxidized
453 by O₃ in the troposphere. In OFR254, they can still have significant contributions from O₃ even outside
454 the low-H₂O and/or high-OHR_{ext} conditions.

455 An experimentalist may be interested in obtaining an O_{3exp}/OH_{exp} in an OFR close to ambient values,
456 which requires lower H₂O and higher OHR_{ext} conditions, although care should be taken to avoid other
457 non-tropospheric reactions under those conditions. On the other hand, one may want to study OH-
458 dominated chemistry and thus want to avoid significant ozonolysis of VOCs to reduce the complexity of
459 VOC fate. This is analogous to the addition of excess NO to suppress O₃ in some chamber experiments.
460 In this case the OFRs should be operated under opposite conditions, i.e., high H₂O, high UV, and low
461 OHR_{ext}. This strategy enhancing OH_{exp} is effective for most VOCs, except those with the highest k_{O3}/k_{OH}
462 ratios, e.g., α-terpinene and β-caryophyllene. To further decrease the importance of reactions of VOC
463 with O₃, it is necessary to lower the O₃ concentration. For OFR254, one can inject less O₃ into the reactor

464 and increase the UV lamp setting. The comparison between OFR254-70 and OFR254-7 in Fig. S5
465 demonstrates this approach. For OFR185, we propose another strategy, i.e., lowering O₂ concentration
466 in the reactor. This decreases O₃ production but affects OH production to a much lesser extent, thanks
467 to the major OH production by H₂O photolysis. We simulate the OFR185 cases with 2‰ O₂ and observe
468 that VOC ozonolysis can be excluded at high H₂O and high UV (Fig. S5).

469 Among the literature OFR studies, the field studies employing OFRs in urban and forested areas all
470 operated under O_{3exp}/OH_{exp} values 100 times lower than in the atmosphere. In these field studies
471 reaction of almost all VOCs with O₃ can be neglected, except for the most reactive biogenics with O₃,
472 e.g., α-terpinene and β-caryophyllene. The source study in an urban tunnel of Tkacik et al. (2014)
473 operated under similar conditions. Some laboratory studies using OFR254 (Kang et al., 2011; Lambe et
474 al., 2011b) as well as the biomass smoke source study (Ortega et al., 2013) operated at O_{3exp}/OH_{exp} close
475 to tropospheric values, because the injected O₃ plays a key role for OFR254 studies and the biomass
476 smoke experiments were conducted at high OHR_{ext}. Nevertheless, only α-pinene and β-pinene, both
477 biogenics, are significantly consumed by O₃. Another OFR254 study, Klems et al. (2015), had O_{3exp}/OH_{exp}
478 significant lower than tropospheric values, since the initial O₃ in their experiment was only 2 ppm, and
479 the UV light in their experiment was stronger than our lamps' highest setting and further reduced
480 effective O₃.

481 3.1.6 Reactions with ¹O₂ and HO₂

482 Singlet oxygen, ¹O₂, can be produced in various ways in OFRs (Calvert et al., 2002; Ono et al., 2014)
483 and react with alkenes at appreciable rate constants (~10⁻¹⁷–10⁻¹⁴ cm³ molecule⁻¹ s⁻¹; Huie and Herron,
484 1973; Eisenberg et al., 1986). We estimate ¹O₂ concentration by the expression proposed by Ono et al.
485 (2014). Only at the lowest H₂O, the highest lamp setting, and the highest OHR_{ext} in this study (Table 1),
486 may the most reactive alkene (endo-cyclic conjugated dienes, e.g., cyclopentadiene, α-terpinene, and
487 α-phellandrene) have >10% contribution from ¹O₂ to their fate. For all other species and under all other
488 conditions, reactions of VOCs with ¹O₂ are negligible. Thus, this reactant is not discussed further in the
489 present work.

490 HO₂ is a major radical in the OFR chemistry. However, it is much less reactive than OH toward VOCs.
491 Typically, the rate constants of reactions of HO₂ with alkenes are smaller than 10⁻²⁰ cm³ molecule⁻¹ s⁻¹ at
492 room temperature, and those with almost all saturated VOCs (except aldehydes and ketones) are even
493 smaller (Tsang, 1991; Baulch et al., 1992, 2005). Therefore, we briefly discuss reactions of HO₂ with
494 aldehydes and ketones, and neglect those with all other VOCs in this study. Ketones react with HO₂ at
495 rate constants on the order of 10⁻¹⁶ cm³ molecule⁻¹ s⁻¹ or lower (Gierczak and Ravishankara, 2000; Cours
496 et al., 2007). Therefore, only at low H₂O, low UV and high OHR_{ext}, the reaction of acetone with HO₂ may
497 compete with that with OH. The same is likely true for the reactions of acetaldehyde and larger
498 aldehydes with HO₂, as their rate constants are likely to be around or less than 1x10⁻¹⁴ cm³ molecule⁻¹ s⁻¹
499 ¹ (da Silva and Bozzelli, 2009). Formaldehyde is the only stable carbonyl compound that may react with
500 HO₂ (rate constant: 7.9x10⁻¹⁴ cm³ molecule⁻¹ s⁻¹; Ammann et al., 2015) at a rate competing with that
501 with OH under conditions that are not low-H₂O, low-UV, and high-OHR_{ext}. Note that the reaction of

502 formaldehyde with HO₂ is also significant in the atmosphere (Pitts and Finlayson, 1975; Gäb et al., 1985).
503 However, its product, hydroxymethylperoxy radical, dominantly undergoes decomposition via thermal
504 reaction and photolysis (Kumar and Francisco, 2015), compared to the hydroxymethylhydroperoxide
505 formation pathway via a further reaction with HO₂ (Ziemann and Atkinson, 2012). Even if
506 hydroxymethylhydroperoxide is produced in appreciable amounts, in the high-OH environment of OFRs,
507 this species can be easily predicted to convert into formic acid (Francisco and Eisfeld, 2009) and
508 eventually CO₂. All these products have very few interactions with other VOCs, and hence should not
509 significantly perturb the reaction system of OFRs.

510 **3.1.7 Overall contribution of non-OH reactants to gas-phase chemistry**

511 In this section we summarize the combined effect of all non-OH reactants to VOC consumption.
512 However, we can no longer use $X_{\text{exp}}/\text{OH}_{\text{exp}}$ to express total non-OH VOC consumption as for individual
513 reactants. Total non-OH VOC consumption is thus discussed case by case.

514 In the explored range of conditions (i.e., H₂O, UV, OHR_{ext}, and initial O₃ for OFR254), there are
515 obviously conditions where all non-OH fates of VOCs are negligible. Most simply, the highest H₂O and
516 UV in this study and a very small non-zero OHR_{ext} result in a VOC consumption nearly 100% by OH,
517 regardless of the VOC type (Table S6). Lowering UV can make non-OH contribution even smaller for
518 OFR185, but not for OFR254. This difference occurs because OH production is reduced while O₃ roughly
519 remains at the same level in OFR254, leading to enhanced relative contribution from O₃ to the fate of
520 biogenics. At the lowest non-zero UV in Li et al. (2015)'s PAM reactor (7.9×10^{11} photons cm⁻² s⁻¹ at 185
521 nm; 2.0×10^{14} photons cm⁻² s⁻¹ at 254 nm), the fractional destructions of α-pinene (representative of
522 biogenic VOCs) by O₃ are 21% and 4.2% in OFR254-70 and OFR254-7, respectively. Other OFR designs
523 may reach lower UV, e.g., the "low UV" case defined in this study (1.0×10^{11} photons cm⁻² s⁻¹ at 185 nm;
524 4.2×10^{13} photons cm⁻² s⁻¹ at 254 nm). At these UV levels, the fate of α-pinene by O₃ further increases to
525 44% and 13% in OFR254-70 and OFR254-7, respectively.

526 On the other hand, non-OH reactants can dominate VOC fate under opposite conditions that lead
527 to low OH production and strong OH suppression. At the lowest H₂O and UV and the highest OHR_{ext} in
528 this study, >95% of α-pinene and ~80% of toluene are consumed by non-OH reactants in OFR185. In
529 OFR254, almost all α-pinene has non-OH fate while non-OH fate of toluene is still minor or negligible. If
530 OFRs are operated at the low UV setting from Li et al. (2015)'s PAM, ~8 times higher the lowest UV in
531 this study, the situation hardly changes, as a very large OH suppression persists. Nevertheless, if UV is
532 increased to the highest level, non-OH fate of α-pinene is lowered to ~60–70% and that of toluene in
533 OFR185 decreases to 24%. When H₂O is at the highest level, non-OH fate is systematically lower than at
534 low H₂O in all types of OFRs. In particular, Case HHV has non-OH fates of α-pinene only up to ~10% and
535 negligible non-OH fates of toluene, despite very high OHR_{ext}.

536 We also summarize VOC fate for key laboratory, source, and field studies examined in the present
537 work in Fig. 7. For each case, the fate of one or a few typical VOCs is investigated. In laboratory studies,
538 Kang et al. (2011) performed experiments with a mixture of α-pinene, m-xylene, and p-xylene, and one
539 of Lambe et al. (2011b)'s experiments used biogenics (α-pinene and isoprene, respectively) as

540 precursors. In both cases, O_3 plays a role in the fate of biogenics when H_2O is low (Kang et al.), or OHR_{ext}
541 is high and UV is low (Lambe et al.), as shown in Fig. 7. The fate of isoprene by O_3 is less significant
542 despite the very high OHR_{ext} , because isoprene, compared to α -pinene, is more reactive with OH and
543 less reactive with O_3 . Besides, $O(^3P)$ contributes up to a few percent to the fate of biogenics. In the
544 literature experiments performed at a higher H_2O (Kang et al.) or a higher UV (Lambe et al.), non-OH
545 fate of both VOCs significantly decreases because of increases in OH_{exp} . About 20% of p-xylene in Kang
546 et al.'s mixture experiment at very low H_2O may be destroyed by 254 nm photons, under the assumption
547 of unity quantum yield. Other laboratory study cases with aromatics have lower non-OH fates because
548 of higher H_2O . n-decane in one of Lambe et al.'s experiments and dodecanoic acid in Klems et al. (2015)'s
549 study are consumed $\sim 100\%$ by OH, as these alkane(-like) species neither react rapidly with O_3 , nor
550 absorb UV efficiently. However, as previously discussed, some carbonyl compounds may be formed and
551 significantly photolyzed at 254 nm in Klems et al.'s experiments, although the huge complexity of
552 intermediates and limited knowledge of reaction mechanisms prevents a quantitative assessment of
553 the fate of carbonyl intermediates by photons at 254 nm.

554 Source and field studies usually have highly complex precursors. For the urban tunnel study (Tkacik
555 et al., 2014) and the CalNex-LA study in the Los Angeles basin (Ortega et al., 2015), we choose toluene
556 as a representative of aromatic species, as these are major anthropogenic VOCs and SOA precursors in
557 urban environment (Dzepina et al., 2009; Borbon et al., 2013; Hayes et al., 2015; Jathar et al., 2015).
558 Although alkanes are also major anthropogenic VOCs, their non-OH fate is not quantitatively assessed
559 for the same reason as discussed for dodecanoic acid in Klems et al. (2015)'s experiment. For the smoke
560 aging study, FLAME-3 (Ortega et al., 2013), we select benzene and α -pinene, which are important VOCs
561 in biomass burning emissions (Warneke et al., 2011). For the BEACHON-RoMBAS and SOAS studies at
562 forested sites, α -pinene and isoprene are chosen, respectively, as they are major emitted biogenic VOCs
563 at those corresponding sites. Both the urban tunnel and FLAME-3 studies have aromatic precursors
564 significantly photolyzed at 185 and 254 nm (assuming quantum yield = 1) under the conditions of high
565 source concentrations (Fig. 7). The toluene fate by UV in the tunnel study is less substantial than that of
566 benzene in FLAME-3, since NO_x , the largest fraction of external OH reactant in the tunnel study, is
567 converted into HNO_3 very rapidly (Li et al., 2015) and does not further suppress OH. In the cases of lower
568 OHR_{ext} (e.g., the tunnel experiments with low source concentration and CalNex), toluene is dominantly
569 consumed by OH. It also holds for biogenic VOCs that non-OH fate decreases with decreasing OHR_{ext}
570 due to less OH suppression. The non-OH fate of α -pinene in FLAME-3, dominated by reaction with O_3 ,
571 is larger than 20%, while the non-OH fates of α -pinene in BEACHON-RoMBAS and of isoprene in SOAS
572 are both negligible, since OHR_{ext} in the former study is >10 times higher than in the latter two studies.

573 3.2 SOA photolysis

574 Recently, photolysis in the UV range has been found to be a potentially significant sink of some
575 types SOA in the troposphere (Updyke et al., 2012; Lambe et al., 2013; Liu et al., 2013, 2015; Hodzic et
576 al., 2015; Wong et al., 2015; Romonosky et al., 2016). It is necessary to also investigate SOA photolysis
577 in OFRs, as photons used in OFRs are highly energetic and non-tropospheric. UV extinction due to

578 aerosol optical scattering and in-particle absorption under OFR conditions is generally negligible (Hodzic
579 et al., 2015). For simplicity, we estimate photodegradation ratios of various SOA component surrogates
580 as well as several SOA samples whose absorptivity was measured in previous studies (Updyke et al.,
581 2012; Lambe et al., 2013; Liu et al., 2013; Romonosky et al., 2016) (Fig. 8) under the assumption of unity
582 quantum yield to obtain upper limits of photodegradation ratios, and also under the assumption of
583 lower (0.1 and 0.01) quantum yields.

584 Most SOA functional groups are oxygenated (e.g., peroxides, carbonyls, carboxylic acids, alcohols).
585 The absorption cross sections of most of these functional groups are too low at 185 and 254 nm given
586 the OFR residence time and UV light intensity, leading to a small contribution of photolysis to SOA
587 degradation (Fig. 8). For example, glycolaldehyde has a negligible fractional contribution of photolysis
588 except at the highest lamp setting, when only ~5% of this species photolyzes at each wavelength.
589 Species (e.g., isoprene) with conjugated double bonds as efficient chromophores will not be present in
590 SOA because of their high reactivity with OH and O₃. Nitrate groups may have a ~30% contribution from
591 photolysis at the highest UV settings, and a negligible contribution at intermediate or low UV settings.

592 Aromatic rings are more resistant to OH attack and usually strongly absorb UV light. Under our
593 assumptions, the photolysis of some aromatic SOA components (e.g., o-cresol at 185 nm and
594 naphthalene at 254 nm) is already important at medium UV flux. At the highest lamp setting, most
595 aromatics in SOA would be destroyed if the quantum yields are indeed near unity. However, as
596 previously discussed, photolysis quantum yields of aromatics may be significantly lower than 1. This is
597 more probable in the condensed phase (Damschen et al., 1978; Baker et al., 2015) than in the gas phase,
598 as quenching processes in the condensed-phase matrix are usually much more efficient than through
599 gas-phase molecular collisions. It has recently been reported that photolysis quantum yields of
600 aromatics in SOA were low under UVB irradiation (Romonosky et al., 2015). Although the range and
601 relevance of the species investigated in that study are limited, it is reasonable to assume low quantum
602 yield for aromatic photolysis in SOA at 185 and 254 nm.

603 Wong et al. (2015) conducted α -pinene-derived SOA photolysis experiments in a chamber under
604 UVB irradiation (down to 284 nm). They observed at 85% RH ~30% SOA photolyzed after >30 min
605 irradiation and a photolysis quantum yield of ~1 during the first 10 min. However, in OFRs such a high
606 SOA photodegradation percentage would not occur, since Wong et al. (2015)'s experiments had a high
607 photon flux ($\sim 4 \times 10^{15}$ photons cm⁻² s⁻¹) and a long irradiation time, and hence a photon flux exposure
608 that is ~5 times that at the highest lamp setting in the OFRs modeled in our work. According to the
609 measurements of Wong et al. (2015), a photolysis fraction of ~6% would be expected for this type of
610 SOA in our OFRs under the highest UV flux, with lower percentages at lower UV settings. In addition,
611 the approximate unity quantum yield observed in Wong et al. (2015) may be due to (hydro)peroxides in
612 α -pinene-derived SOA, since peroxides have high photolysis quantum yields (Goldstein et al., 2007;
613 Epstein et al., 2012), while other functional groups (i.e., mainly hydroxyl and carbonyl) in oxygenated
614 species in SOA are unlikely to have for reasons discussed below.

615 Note that a simple addition of absorptivities of different functional groups may not explain SOA

616 absorptivity (Phillips and Smith, 2015). According to the absorption data of SOA samples from Lambe et
617 al. (2013) and Romonosky et al. (2015a), real SOA absorbs $\sim 1\text{--}3$ orders of magnitude more than non-
618 aromatic component surrogate species shown in Fig. 8 at 254 nm. As discussed for multifunctional
619 oxidation intermediates (with carbonyls and hydroxyls), SOA absorption enhancement may be largely
620 due to transitions of charge transfer complexes formed between carbonyls and hydroxyls in
621 multifunctional oxygenated SOA components (Phillips and Smith, 2014, 2015). These complexes
622 between carbonyls and hydroxyls also have continua of states likely leading to ultrafast relaxation and
623 hence low photolysis quantum yields. Charge transfer transitions have been extensively shown in
624 measurements (Alif et al., 1991; Gao and Zepp, 1998; Johannessen and Miller, 2001; O'Sullivan et al.,
625 2005; Zhang et al., 2006; Osburn et al., 2009; Sharpless and Blough, 2014) to have very low quantum
626 yields in the condensed phase. Sharpless and Blough (2014) compiled quantum yields of various
627 products of humic-like matter photolysis down to 280 nm. No quantum yields except those of the
628 product $^1\text{O}_2$, which is generally unimportant for OFRs (see Section 3.1.6), are higher than 0.01. If the
629 photolysis quantum yields of the SOA samples in Fig. 8 at 254 nm are no more than 0.01, no SOA samples
630 will be photolyzed by 20% even at the highest OFR lamp setting, and photolysis of most SOA samples at
631 254 nm will be minor or negligible in OFRs. Thus, to our current knowledge, lack of solid information on
632 quantum yields of SOA components with multiple carbonyls and hydroxyls at 254 nm prevents a clear
633 assessment of SOA photolysis in OFRs at the medium and high UV. On the other hand, direct
634 measurements are desirable for this issue and caution should still be exercised for OFR experiments at
635 relatively high UV.

636 SOA photolysis at 185 nm may be lower compared to that at 254 nm. SOA absorptivity data at 185
637 nm are not available. According to SOA mass-specific absorption cross-section (MAC) data between 250
638 and 300 nm in Romonosky et al. (2015a), there is a linear relationship between the logarithm of MAC
639 and wavelength for most SOA samples: MAC increases by a factor of ~ 3 per 50 nm decrease in
640 wavelength. We thus extrapolate this relationship to 185 nm, where MAC is estimated to be ~ 3.5 times
641 higher than that at 254 nm. However, the UV flux at 185 nm in our OFR is ~ 100 times lower than at 254
642 nm.

643 Based on the discussion above, the SOA photodegradation ratio of $\sim 30\%$ in Wong et al. (2015)'s
644 non-OFR setup may be explained. α -pinene-derived SOA has $\sim 20\text{--}50\%$ weight fraction of peroxides
645 (Docherty et al., 2005; Epstein et al., 2014), which may undergo photolysis in SOA to convert into
646 carbonyls (and hydroxyls) (Epstein et al., 2014). We speculate that after the formation of carbonyls from
647 peroxides, SOA materials cannot proceed significantly further with photolysis as discussed for charge
648 transfer between carbonyl and hydroxyl above. In the experiments of Wong et al. (2015), as well as
649 Epstein et al. (2014), effective photolysis rate constants/quantum yields decreased as SOA photolysis
650 proceeded. Photolysis rates were substantially reduced after a $\sim 30\%$ mass loss due to photolysis in
651 Wong et al. (2015)'s experiments. This mass loss ratio is consistent with the mass percentage of
652 peroxides in α -pinene-derived SOA. Again, we note that, according to the extrapolation from Wong et
653 al. (2015)'s results, the mass loss percentage expected in our OFR under the highest UV flux is $\sim 6\%$ for

654 α -pinene-derived SOA. This value is much lower than that shown in Fig. 8 under the assumption of unity
655 quantum yield (~40%) because of a substantially decreasing quantum yield in the real photolysis
656 experiments. Therefore, in OFRs, even if (hydro)peroxides in SOA may be photolyzed in appreciable
657 amounts, SOA mass is unlikely to be largely destroyed by photons in OFRs, as (hydro)peroxides may
658 convert into carbonyls and hydroxyls, which may substantially lower subsequent photolysis quantum
659 yields.

660 According to the discussion above, measurements of quantum yields and/or products of SOA
661 photolysis are highly desirable, especially for the photolysis of SOA containing dominantly carbonyl and
662 hydroxyl groups, as (hydro)peroxides, which are likely to form in OFRs, may convert into hydroxyls and
663 carbonyls. With more data on quantum yields of SOA photolysis, a clearer strategy for including or
664 excluding SOA photolysis in OFRs can be made.

665 Even though SOA photolysis can be significant in OFRs, it only proceeds to a much lesser extent
666 compared to ambient SOA photolysis. We calculate the numbers of e-fold decay of SOA photolysis in
667 OFR254-70 and the troposphere according to the effective ambient photolysis lifetime of SOA from
668 Romonosky et al. (2015a). Under the condition of 70% RH ($H_2O = 1.4\%$) and $OHR_{ext} = 25\ s^{-1}$ (typical of
669 ambient conditions), SOA samples are estimated to undergo ~0.01–0.5 e-fold photolysis timescales (i.e.,
670 ~1–35% OA photolyzed) in OFR254-70 at an equivalent photochemical age of 1 week under the upper
671 limit assumption of unity quantum yields (Table S8). However, in the atmosphere, those samples may
672 proceed with 10^2 – 10^4 e-fold decays of photolysis (i.e., virtually complete destruction) at the same
673 photochemical age, if ambient SOA photolysis quantum yields are assumed to be those of H_2O_2 (unity
674 below 400 nm). Even if the quantum yield of acetone (non-zero below 320 nm, see Romonosky et al.,
675 2015a) is taken as a surrogate for SOA, most types of SOA would still be completely or nearly completely
676 photolyzed under ambient conditions. These results demonstrate that ambient SOA photolysis is likely
677 to be much more important than in OFRs. On the other hand, they also highlight the need for studies
678 of ambient SOA photolysis quantum yields and photolytic aging, as ambient SOA is unlikely to be
679 completely destroyed by photons within only 1 week. Either their quantum yields are much lower than
680 used in this study, or the photolabile groups are destroyed and leave behind others that are not (or less)
681 photolabile during photolytic aging.

682 **3.3 Guidelines for OFR experimental design and operation**

683 It is necessary to avoid significant non-tropospheric chemistry in OFRs in order to more accurately
684 simulate tropospheric aging. Only photolysis at 185 and 254 nm are important non-tropospheric
685 pathways in OFRs and reactions with O atoms are generally unimportant. Ozonolysis is also a major VOC
686 sink in the troposphere, and the desirability of including or excluding its effects depends on the goals of
687 each experiment.

688 In the cases where the exclusion of VOC ozonolysis is desired, there is no dilemma for the
689 experimental design, as the exclusion of both VOC ozonolysis and non-tropospheric VOC consumption
690 requires similar conditions, i.e., safer conditions. As shown above, all examined field studies do not have
691 significant non-tropospheric contribution to VOC fate, while some past laboratory and source studies

692 do because of low H₂O and/or very high OHR_{ext} in those experiments. It is possible to improve the latter
693 experiments by increasing H₂O and/or lowering OHR_{ext}. In detail, source humidification and dilution can
694 be feasible measures to increase H₂O and decrease OHR_{ext}, respectively. For example, increasing RH
695 from 3% to 60% (H₂O from ~0.06% to ~1.2%) lowers the percentage of non-tropospheric consumption
696 of p-xylene in Kang et al. (2011)'s mixture experiment from ~20% to 1.5%. Humidifying the average
697 condition of the BEACHON-RoMBAS (Palm et al., 2015) campaign from H₂O = 1.6% (RH = 63%) to H₂O =
698 2.3% (RH = 92%) leads to significant (from ~20% for 185 nm photon flux to a factor of ~3 for O(³P))
699 decreases in all exposure ratios between non-OH reactants and OH (Table S4). Also, a 5-fold source
700 dilution in FLAME-3 reduces the non-tropospheric fate of benzene from >60% to ~15% (Table S4 and
701 "Improved" cases in Fig. 7). Injecting less precursor is a simple way to keep a reasonably low OHR_{ext} in
702 laboratory studies. The comparison between the cases with high and low concentrations in the urban
703 tunnel study (Tkacik et al., 2014) is a good example (Table S4 and Fig. 7). Note that when taking the
704 measures above to limit non-tropospheric VOC fate, one generally reduces the contribution from all
705 non-OH reactants. Increasing H₂O and source dilution also significantly lower the relative importance of
706 ozonolysis in the fate of α-pinene in Kang et al.'s mixture experiments and the FLAME-3 study (Table S4
707 and Fig. 7). Although increasing UV may increase OH production, OH reactant destruction, and hence
708 the relative contribution of OH to VOC fate in some cases, one has to be cautious when taking this
709 measure to reduce effective OHR_{ext}, as high UV may cause non-tropospheric photolysis of aromatic SOA
710 components.

711 In laboratory experiments, running OFRs under safer conditions ensures a minor contribution of
712 non-tropospheric photolysis, based on the current knowledge of oxidation intermediate photolysis (Fig.
713 2). This also reduces the relative contribution of ozonolysis to VOC fate. However, when more
714 information becomes available about photolysis quantum yields of oxidation intermediates (vs. the
715 upper limits assumed here), there may be additional flexibility to include ozonolysis while excluding
716 non-tropospheric VOC consumption. As the precursor composition is usually relatively simple in
717 laboratory experiments, it is sufficient to ensure the insignificance of non-tropospheric consumption of
718 only the precursor(s) and possible intermediates (usually oxygenated species), rather than for a large
719 variety of VOC precursors and intermediates. For example, in the case of quantum yields significantly
720 lower than used in the present work, we may perform OFR254-70 experiments with a large amount of
721 biogenics at medium H₂O and UV. In this case, a tropospheric O_{3exp}/OH_{exp} ratio can be obtained without
722 major side effects, because the fractional contribution of photolysis of possible intermediates is still
723 minor due to low quantum yields. On the other hand, OFR experiments with some anthropogenic VOCs,
724 such as alkanes, can just be conducted at high H₂O and low OHR_{ext} to avoid the contribution of all non-
725 OH reactants, since ozonolysis of alkanes is negligible even at a tropospheric O_{3exp}/OH_{exp}.

726 OFR experiments can be simply conducted under safer conditions to avoid non-tropospheric VOC
727 fate, while riskier conditions can lead to significant non-tropospheric VOC fate, depending on the
728 species under study. The conditions in between, i.e., "transition" conditions, are explicitly discussed
729 above. However, one may want to be able to more quantitatively estimate the relative importance of

730 non-OH reactants under different conditions so that a more detailed experimental planning becomes
731 possible that simultaneously ensures insignificant non-tropospheric VOC fate and specific experimental
732 goals. For this purpose, we provide a series of estimation equations for non-OH reactant exposures
733 (Section S3, Table S9, and Fig. S6, as well as Excel file). With these equations, the relative contribution
734 of non-OH reactants under all conditions explored in this study can be easily estimated. In OFR studies
735 where a different OFR design is adopted and/or chemistry beyond the approximations in our model is
736 involved, a new model may need to be established, which can be done in similar manner as Peng et al.
737 (2015), to obtain the relative importance of non-OH VOC fate and then perform experimental design.

738 **4 Conclusions**

739 We used a kinetic model to investigate non-OH contribution (from 185 and 254 nm photons, $O(^1D)$,
740 $O(^3P)$, and O_3) to VOC destruction, as well as to SOA photolysis at 185 and 254 nm in OFRs. We assessed
741 the relative significance of the VOC consumption by non-OH reactants to that by OH in OFRs and the
742 troposphere. The only non-tropospheric reaction that can play a major role under OFR conditions is
743 photolysis, especially at 254 nm. The relative importance of photolysis is largest under riskier OFR
744 conditions where OH is low due to low H_2O and/or high OHR_{ext} . Due to lack of quantum yield data, we
745 estimated upper limits of the relative importance of photolysis for the few most susceptible oxidation
746 intermediates, which are comparable to those from aromatic precursors. Reactions of O atoms are not
747 competitive and are actually of lower relative importance (vs. OH) in OFRs than in the troposphere. VOC
748 ozonolysis is much less important than in the troposphere under typical OFR conditions and of similar
749 importance under riskier OFR conditions. Photolysis of SOA in OFRs could be significant at medium and
750 high UV, but only if corresponding quantum yields are high. If SOA photolysis quantum yields are of the
751 order of 0.01 or lower, as measured for many humic-like substances (Sharpless and Blough, 2014), SOA
752 photolysis in OFRs may be minor or negligible under most conditions. Although the reaction fates may
753 be different, numbers of e-fold decays of photolysis for a given OH_{exp} are at least an order-of-magnitude
754 lower in the OFRs compared to the troposphere.

755 We examined some past field, laboratory, and source studies using OFRs. In the field studies of
756 aged urban and forest ambient air, non-OH VOC fate was not important because of relatively high H_2O
757 and moderate OHR_{ext} . However, some laboratory and source studies were conducted at low H_2O and/or
758 high OHR_{ext} , and have significant non-tropospheric VOC consumption. Humidification and/or dilution
759 are recommended in these cases to reduce the importance of non-tropospheric reactants. We proposed
760 different approaches to avoid non-OH VOC consumption, as well as strategies to employ insignificant
761 non-tropospheric photolysis and significant tropospheric ozonolysis simultaneously in laboratory
762 experiments. Our work has implications for the interpretation of past OFR studies, and should be useful
763 for designing and conducting future OFR experiments for atmospheric research, as well as in related
764 applied fields.

765 The need for systematic measurements of photolysis quantum yields, for both VOC and SOA, and
766 both at actinic wavelengths and at 185 and 254 nm, was highlighted in this study. When quantum yield
767 data become available, photolysis of oxidation precursors, oxidation intermediates, and SOA in OFRs

768 can be much better quantified, its relative importance compared to OH oxidation, ambient photolysis
769 etc. can be better evaluated, and experimental planning might then be able to be less conservative and
770 have more freedom to avoid non-tropospheric photolysis and realize specific experimental objective(s).

771

772 **Acknowledgements**

773 We thank Veronica Vaida, Paul Ziemann, Andrew Lambe, and the PAM user community for useful
774 discussions, Andrew Lambe and Daniel Tkacik for providing some OFR experimental data, and the
775 reviewers for their useful comments for improving the manuscript. This research was partially
776 supported by CARB 11-305, DOE (BER/ASR) DE-SC0011105, NSF AGS-1243354 & AGS-1360834, and
777 NASA NNX15AT96G. AMO acknowledges fellowships from DOE and CU Graduate School. RL and BBP
778 acknowledge CIRES Fellowships. BBP is grateful for a Fellowship from US EPA STAR (FP-91761701-0).
779 Resources supporting this work were provided by the NASA High-End Computing (HEC) Program
780 through the NASA Center for Climate Simulation (NCCS) at Goddard Space Flight Center.

781

782 **References**

- 783 Aimanant, S. and Ziemann, P. J.: Chemical Mechanisms of Aging of Aerosol Formed from the Reaction
784 of n-Pentadecane with OH Radicals in the Presence of NO_x, *Aerosol Sci. Technol.*, 47(9), 979–990,
785 doi:10.1080/02786826.2013.804621, 2013.
- 786 Alif, A., Pilichowski, J. and Boule, P.: photochemistry and environment XIII phototransformation of 2-
787 nitrophenol in aqueous solution, *J. Photochem. Photobiol. A Chem.*, 59, 209–219, doi:10.1016/1010-
788 6030(91)87009-K, 1991.
- 789 Ammann, M., Cox, R. A., Crowley, J. N., Jenkin, M. E., Mellouki, A., Rossi, M. J., Troe, J., Wallington, T. J.,
790 Cox, B., Atkinson, R., Baulch, D. L. and Kerr, J. A.: IUPAC Task Group on Atmospheric Chemical Kinetic
791 Data Evaluation, [online] Available from: <http://iupac.pole-ether.fr/#>, 2015.
- 792 Atkinson, R. and Arey, J.: Atmospheric degradation of volatile organic compounds., *Chem. Rev.*, 103(12),
793 4605–38, doi:10.1021/cr0206420, 2003.
- 794 Bahreini, R., Middlebrook, A. M., Brock, C. A., de Gouw, J. A., McKeen, S. A., Williams, L. R., Daumit, K.
795 E., Lambe, A. T., Massoli, P., Canagaratna, M. R., Ahmadov, R., Carrasquillo, A. J., Cross, E. S., Ervens, B.,
796 Holloway, J. S., Hunter, J. F., Onasch, T. B., Pollack, I. B., Roberts, J. M., Ryerson, T. B., Warneke, C.,
797 Davidovits, P., Worsnop, D. R. and Kroll, J. H.: Mass spectral analysis of organic aerosol formed downwind
798 of the Deepwater Horizon oil spill: field studies and laboratory confirmations., *Environ. Sci. Technol.*,
799 46(15), 8025–34, doi:10.1021/es301691k, 2012.
- 800 Baker, L. a., Horbury, M. D., Greenough, S. E., Coulter, P. M., Karsili, T. N. V., Roberts, G. M., Orr-Ewing, A.
801 J., Ashfold, M. N. R. and Stavros, V. G.: Probing the Ultrafast Energy Dissipation Mechanism of the
802 Sunscreen Oxybenzone after UVA Irradiation, *J. Phys. Chem. Lett.*, 6, 1363–1368,
803 doi:10.1021/acs.jpcclett.5b00417, 2015.
- 804 Baulch, D. L., Bowman, C. T., Cobos, C. J., Cox, R. A., Just, T., Kerr, J. A., Pilling, M. J., Stocker, D., Troe, J.,
805 Tsang, W., Walker, R. W. and Warnatz, J.: Evaluated kinetic data for combustion modeling: Supplement
806 II, *J. Phys. Chem. Ref. Data*, 34(3), 757–1397, doi:10.1063/1.1748524, 2005.
- 807 Baulch, D. L., Cobos, C. J., Cox, R. A., Esser, C., Frank, P., Just, T., Kerr, J. A., Pilling, M. J., Troe, J., Walker,
808 R. W. and Warnatz, J.: Evaluated Kinetic Data for Combustion Modelling, *J. Phys. Chem. Ref. Data*, 21(3),
809 411, doi:10.1063/1.555908, 1992.
- 810 Beddard, G. S., Fleming, G. R., Gijzeman, O. L. J. and Porter, G.: Vibrational Energy Dependence of
811 Radiationless Conversion in Aromatic Vapours, *Proc. R. Soc. A Math. Phys. Eng. Sci.*, 340(1623), 519–533,
812 doi:10.1098/rspa.1974.0168, 1974.
- 813 Borbon, A., Gilman, J. B., Kuster, W. C., Grand, N., Chevaillier, S., Colomb, A., Dolgorouky, C., Gros, V.,
814 Lopez, M., Sarda-Estevé, R., Holloway, J., Stutz, J., Petetin, H., McKeen, S., Beekmann, M., Warneke, C.,
815 Parrish, D. D. and De Gouw, J. A.: Emission ratios of anthropogenic volatile organic compounds in
816 northern mid-latitude megacities: Observations versus emission inventories in Los Angeles and Paris, *J.*
817 *Geophys. Res. Atmos.*, 118(4), 2041–2057, doi:10.1002/jgrd.50059, 2013.
- 818 Bouzidi, H., Aslan, L., El Dib, G., Coddeville, P., Fittschen, C. and Tomas, A.: Investigation of the Gas-Phase
819 Photolysis and Temperature-Dependent OH Reaction Kinetics of 4-Hydroxy-2-butanone, *Environ. Sci.*
820 *Technol.*, 49(20), 12178–12186, doi:10.1021/acs.est.5b02721, 2015.
- 821 Bouzidi, H., Laversin, H., Tomas, a., Coddeville, P., Fittschen, C., El Dib, G., Roth, E. and Chakir, a.:
822 Reactivity of 3-hydroxy-3-methyl-2-butanone: Photolysis and OH reaction kinetics, *Atmos. Environ.*,
823 98(3), 540–548, doi:10.1016/j.atmosenv.2014.09.033, 2014.
- 824 Calvert, J. G., Atkinson, R., Becker, K. H., Kamens, R. M., Seinfeld, J. H., Wallington, T. H. and Yarwood,
825 G.: *The Mechanisms of Atmospheric Oxidation of the Aromatic Hydrocarbons*, Oxford University Press,
826 USA. [online] Available from: <https://books.google.com/books?id=P0basaLrxDMC>, 2002.
- 827 Carlton, A. G., Wiedinmyer, C. and Kroll, J. H.: A review of Secondary Organic Aerosol (SOA) formation
828 from isoprene, *Atmos. Chem. Phys.*, 9(14), 4987–5005, doi:10.5194/acp-9-4987-2009, 2009.
- 829 Carter, W. P. L., Cocker, D. R., Fitz, D. R., Malkina, I. L., Bumiller, K., Sauer, C. G., Pisano, J. T., Bufalino, C.
830 and Song, C.: A new environmental chamber for evaluation of gas-phase chemical mechanisms and
831 secondary aerosol formation, *Atmos. Environ.*, 39(40), 7768–7788,
832 doi:10.1016/j.atmosenv.2005.08.040, 2005.

833 Cocker, D. R., Flagan, R. C. and Seinfeld, J. H.: State-of-the-Art Chamber Facility for Studying Atmospheric
834 Aerosol Chemistry, *Environ. Sci. Technol.*, 35(12), 2594–2601, doi:10.1021/es0019169, 2001.

835 Cours, T., Canneaux, S. and Bohr, F.: Features of the potential energy surface for the reaction of HO₂
836 radical with acetone, *Int. J. Quantum Chem.*, 107(6), 1344–1354, doi:10.1002/qua.21269, 2007.

837 Cubison, M. J., Ortega, a. M., Hayes, P. L., Farmer, D. K., Day, D., Lechner, M. J., Brune, W. H., Apel, E.,
838 Diskin, G. S., Fisher, J. a., Fuelberg, H. E., Hecobian, a., Knapp, D. J., Mikoviny, T., Riemer, D., Sachse, G.
839 W., Sessions, W., Weber, R. J., Weinheimer, a. J., Wisthaler, a. and Jimenez, J. L.: Effects of aging on
840 organic aerosol from open biomass burning smoke in aircraft and laboratory studies, *Atmos. Chem.*
841 *Phys.*, 11(23), 12049–12064, doi:10.5194/acp-11-12049-2011, 2011.

842 Damschen, D. E., Merritt, C. D., Perry, D. L., Scott, G. W. and Talley, L. D.: Intersystem Crossing Kinetics,
843 *J. Phys. Chem.*, 82(21), 2268–2272, doi:10.1021/j100510a002, 1978.

844 Docherty, K. S., Wu, W., Lim, Y. Bin and Ziemann, P. J.: Contributions of Organic Peroxides to Secondary
845 Aerosol Formed from Reactions of Monoterpenes with O₃, *Environ. Sci. Technol.*, 39(11), 4049–4059,
846 doi:10.1021/es050228s, 2005.

847 Dzepina, K., Volkamer, R. M., Madronich, S., Tulet, P., Ulbrich, I. M., Zhang, Q., Cappa, C. D., Ziemann, P.
848 J. and Jimenez, J. L.: Evaluation of recently-proposed secondary organic aerosol models for a case study
849 in Mexico City, *Atmos. Chem. Phys.*, 9(15), 5681–5709, doi:10.5194/acp-9-5681-2009, 2009.

850 Eisenberg, W. C., Taylor, K. and Murray, R. W.: Gas-Phase Kinetics of the Reaction of Singlet Oxygen with
851 Olefins at Atmospheric Pressure, *J. Phys. Chem.*, 90(20), 1945–1948, doi:10.1021/j100400a041, 1986.

852 Epstein, S. A., Blair, S. L. and Nizkorodov, S. A.: Direct Photolysis of α -Pinene Ozonolysis Secondary
853 Organic Aerosol: Effect on Particle Mass and Peroxide Content, *Environ. Sci. Technol.*, 48(19), 11251–8,
854 doi:10.1021/es502350u, 2014.

855 Epstein, S. A., Shemesh, D., Tran, V. T., Nizkorodov, S. A. and Gerber, R. B.: Absorption Spectra and
856 Photolysis of Methyl Peroxide in Liquid and Frozen Water, *J. Phys. Chem. A*, 116(24), 6068–6077,
857 doi:10.1021/jp211304v, 2012.

858 Evans, R. C., Douglas, P. and Burrow, H. D., Eds.: *Applied Photochemistry*, Springer Netherlands,
859 Dordrecht., 2013.

860 Fang, W. H. and Phillips, D. L.: The crucial role of the S₁/T₂/T₁ intersection in the relaxation dynamics of
861 aromatic carbonyl compounds upon $n \rightarrow \pi^*$ excitation, *ChemPhysChem*, 3(10), 889–892,
862 doi:10.1002/1439-7641(20021018)3:10<889::AID-CPHC889>3.0.CO;2-U, 2002.

863 Foster, R.: *Organic Charge-Transfer Complexes*, Academic Press, New York., 1969.

864 Francisco, J. S. and Seinfeld, W.: Atmospheric Oxidation Mechanism of Hydroxymethyl Hydroperoxide †,
865 *J. Phys. Chem. A*, 113(26), 7593–7600, doi:10.1021/jp901735z, 2009.

866 Gäb, S., Hellpointner, E., Turner, W. V. and Köfte, F.: Hydroxymethyl hydroperoxide and
867 bis(hydroxymethyl) peroxide from gas-phase ozonolysis of naturally occurring alkenes, *Nature*,
868 316(6028), 535–536, doi:10.1038/316535a0, 1985.

869 Gao, H. and Zepp, R. G.: Factors Influencing Photoreactions of Dissolved Organic Matter in a Coastal
870 River of the Southeastern United States, *Environ. Sci. Technol.*, 32(19), 2940–2946,
871 doi:10.1021/es9803660, 1998.

872 George, I. J., Vlasenko, A., Slowik, J. G., Broekhuizen, K. and Abbatt, J. P. D.: Heterogeneous oxidation of
873 saturated organic aerosols by hydroxyl radicals: uptake kinetics, condensed-phase products, and particle
874 size change, *Atmos. Chem. Phys.*, 7(16), 4187–4201, doi:10.5194/acp-7-4187-2007, 2007.

875 Gierczak, T. and Ravishankara, A. R.: Does the HO₂ radical react with ketones?, *Int. J. Chem. Kinet.*, 32(9),
876 573–580, doi:10.1002/1097-4601(2000)32:9<573::AID-KIN7>3.0.CO;2-V, 2000.

877 Goldstein, S., Aschengrau, D., Diamant, Y. and Rabani, J.: Photolysis of Aqueous H₂O₂: Quantum Yield
878 and Applications for Polychromatic UV Actinometry in Photoreactors, *Environ. Sci. Technol.*, 41(21),
879 7486–7490, doi:10.1021/es071379t, 2007.

880 Hallquist, M., Wenger, J. C., Baltensperger, U., Rudich, Y., Simpson, D., Claeys, M., Dommen, J., Donahue,
881 N. M., George, C., Goldstein, A. H., Hamilton, J. F., Herrmann, H., Hoffmann, T., Iinuma, Y., Jang, M.,

882 Jenkin, M. E., Jimenez, J. L., Kiendler-Scharr, A., Maenhaut, W., McFiggans, G., Mentel, T. F., Monod, A.,
883 Prevot, A. S. H., Seinfeld, J. H., Surratt, J. D., Szmigielski, R. and Wildt, J.: The formation, properties and
884 impact of secondary organic aerosol: current and emerging issues, *Atmos. Chem. Phys.*, 9(14), 5155–
885 5236 [online] Available from: <Go to ISI>://WOS:000268535500040, 2009.

886 Hayes, P. L., Carlton, a. G., Baker, K. R., Ahmadov, R., Washenfelder, R. a., Alvarez, S., Rappenglück, B.,
887 Gilman, J. B., Kuster, W. C., de Gouw, J. a., Zotter, P., Prévôt, a. S. H., Szidat, S., Kleindienst, T. E., Offenber,
888 J. H., Ma, P. K. and Jimenez, J. L.: Modeling the formation and aging of secondary organic aerosols in Los
889 Angeles during CalNex 2010, *Atmos. Chem. Phys.*, 15(10), 5773–5801, doi:10.5194/acp-15-5773-2015,
890 2015.

891 Hodzic, A., Madronich, S., Kasibhatla, P. S., Tyndall, G., Aumont, B., Jimenez, J. L., Lee-Taylor, J. and
892 Orlando, J.: Organic photolysis reactions in tropospheric aerosols: effect on secondary organic aerosol
893 formation and lifetime, *Atmos. Chem. Phys.*, 15(16), 9253–9269, doi:10.5194/acp-15-9253-2015, 2015.

894 Hoffmann, T., Odum, J. R., Bowman, F., Collins, D., Klockow, D., Flagan, R. C. and Seinfeld, J. H.:
895 Formation of Organic Aerosols from the Oxidation of Biogenic Hydrocarbons, *J. Atmos. Chem.*, 26(2),
896 189–222, doi:10.1023/A:1005734301837, 1997.

897 Hu, W. W., Campuzano-Jost, P., Palm, B. B., Day, D. A., Ortega, A. M., Hayes, P. L., Krechmer, J. E., Chen,
898 Q., Kuwata, M., Liu, Y. J., de Sá, S. S., McKinney, K., Martin, S. T., Hu, M., Budisulistiorini, S. H., Riva, M.,
899 Surratt, J. D., St. Clair, J. M., Isaacman-Van Wertz, G., Yee, L. D., Goldstein, A. H., Carbone, S., Brito, J.,
900 Artaxo, P., de Gouw, J. A., Koss, A., Wisthaler, A., Mikoviny, T., Karl, T., Kaser, L., Jud, W., Hansel, A.,
901 Docherty, K. S., Alexander, M. L., Robinson, N. H., Coe, H., Allan, J. D., Canagaratna, M. R., Paulot, F. and
902 Jimenez, J. L.: Characterization of a real-time tracer for isoprene epoxydiols-derived secondary organic
903 aerosol (IEPOX-SOA) from aerosol mass spectrometer measurements, *Atmos. Chem. Phys.*, 15(20),
904 11807–11833, doi:10.5194/acp-15-11807-2015, 2015.

905 Huie, R. E. and Herron, J. T.: Kinetics of the reactions of singlet molecular oxygen (O₂1Dg) with organic
906 compounds in the gas phase, *Int. J. Chem. Kinet.*, 5(2), 197–211, doi:10.1002/kin.550050204, 1973.

907 Jathar, S. H., Cappa, C. D., Wexler, a. S., Seinfeld, J. H. and Kleeman, M. J.: Multi-generational oxidation
908 model to simulate secondary organic aerosol in a 3-D air quality model, *Geosci. Model Dev.*, 8(8), 2553–
909 2567, doi:10.5194/gmd-8-2553-2015, 2015.

910 Johannessen, S. C. and Miller, W. L.: Quantum yield for the photochemical production of dissolved
911 inorganic carbon in seawater, *Mar. Chem.*, 76(4), 271–283, doi:10.1016/S0304-4203(01)00067-6, 2001.

912 Johnson, M. S., Nilsson, E. J. K., Svensson, E. A. and Langer, S.: Gas-Phase Advanced Oxidation for
913 Effective, Efficient in Situ Control of Pollution, *Environ. Sci. Technol.*, 48(15), 8768–8776,
914 doi:10.1021/es5012687, 2014.

915 Kang, E., Root, M. J., Toohey, D. W. and Brune, W. H.: Introducing the concept of Potential Aerosol Mass
916 (PAM), *Atmos. Chem. Phys.*, 7(22), 5727–5744, doi:10.5194/acp-7-5727-2007, 2007.

917 Kang, E., Toohey, D. W. and Brune, W. H.: Dependence of SOA oxidation on organic aerosol mass
918 concentration and OH exposure: experimental PAM chamber studies, *Atmos. Chem. Phys.*, 11(4), 1837–
919 1852, doi:10.5194/acp-11-1837-2011, 2011.

920 Keller-Rudek, H., Moortgat, G. K., Sander, R. and Sörensen, R.: The MPI-Mainz UV/VIS Spectral Atlas of
921 Gaseous Molecules of Atmospheric Interest, [online] Available from: [www.uv-vis-spectral-atlas-](http://www.uv-vis-spectral-atlas-mainz.org)
922 [mainz.org](http://www.uv-vis-spectral-atlas-mainz.org), 2015.

923 Klems, J. P., Lippa, K. a and McGivern, W. S.: Quantitative Evidence for Organic Peroxy Radical
924 Photochemistry at 254 nm, *J. Phys. Chem. A*, 119(2), 344–351, doi:10.1021/jp509165x, 2015.

925 Kumar, M. and Francisco, J. S.: Red-Light-Induced Decomposition of an Organic Peroxy Radical: A New
926 Source of the HO₂ Radical, *Angew. Chemie Int. Ed.*, doi:10.1002/anie.201509311, 2015.

927 Kwok, E. and Atkinson, R.: Estimation of hydroxyl radical reaction rate constants for gas-phase organic
928 compounds using a structure-reactivity relationship: An update, *Atmos. Environ.*, 29(14), 1685–1695,
929 doi:10.1016/1352-2310(95)00069-B, 1995.

930 Lambe, A. T., Ahern, A. T., Williams, L. R., Slowik, J. G., Wong, J. P. S., Abbatt, J. P. D., Brune, W. H., Ng, N.
931 L., Wright, J. P., Croasdale, D. R., Worsnop, D. R., Davidovits, P. and Onasch, T. B.: Characterization of
932 aerosol photooxidation flow reactors: heterogeneous oxidation, secondary organic aerosol formation

933 and cloud condensation nuclei activity measurements, *Atmos. Meas. Tech.*, 4(3), 445–461,
934 doi:10.5194/amt-4-445-2011, 2011a.

935 Lambe, A. T., Cappa, C. D., Massoli, P., Onasch, T. B., Forestieri, S. D., Martin, A. T., Cummings, M. J.,
936 Croasdale, D. R., Brune, W. H., Worsnop, D. R. and Davidovits, P.: Relationship between Oxidation Level
937 and Optical Properties of Secondary Organic Aerosol, *Environ. Sci. Technol.*, 47(12), 6349–6357,
938 doi:10.1021/es401043j, 2013.

939 Lambe, A. T., Chhabra, P. S., Onasch, T. B., Brune, W. H., Hunter, J. F., Kroll, J. H., Cummings, M. J., Brogan,
940 J. F., Parmar, Y., Worsnop, D. R., Kolb, C. E. and Davidovits, P.: Effect of oxidant concentration, exposure
941 time, and seed particles on secondary organic aerosol chemical composition and yield, *Atmos. Chem.*
942 *Phys.*, 15(6), 3063–3075, doi:10.5194/acp-15-3063-2015, 2015.

943 Lambe, A. T., Onasch, T. B., Croasdale, D. R., Wright, J. P., Martin, A. T., Franklin, J. P., Massoli, P., Kroll, J.
944 H., Canagaratna, M. R., Brune, W. H., Worsnop, D. R. and Davidovits, P.: Transitions from
945 Functionalization to Fragmentation Reactions of Laboratory Secondary Organic Aerosol (SOA)
946 Generated from the OH Oxidation of Alkane Precursors, *Environ. Sci. Technol.*, 46(10), 5430–5437,
947 doi:10.1021/es300274t, 2012.

948 Lambe, A. T., Onasch, T. B., Massoli, P., Croasdale, D. R., Wright, J. P., Ahern, A. T., Williams, L. R., Worsnop,
949 D. R., Brune, W. H. and Davidovits, P.: Laboratory studies of the chemical composition and cloud
950 condensation nuclei (CCN) activity of secondary organic aerosol (SOA) and oxidized primary organic
951 aerosol (OPOA), *Atmos. Chem. Phys.*, 11(17), 8913–8928, doi:10.5194/acp-11-8913-2011, 2011b.

952 Laue, T. and Plagens, A.: *Named Organic Reactions*, 2nd ed., John Wiley & Sons, Chichester, England,
953 New York. [online] Available from: <http://www.wiley.com/WileyCDA/WileyTitle/productCd-047001041X.html>, 2005.

954

955 Levy II, H.: Normal atmosphere: large radical and formaldehyde concentrations predicted., *Science*,
956 173(3992), 141–143, doi:10.1126/science.173.3992.141, 1971.

957 Li, R., Palm, B. B., Borbon, A., Graus, M., Warneke, C., Ortega, a M., Day, D. a, Brune, W. H., Jimenez, J.
958 L. and de Gouw, J. a: Laboratory Studies on Secondary Organic Aerosol Formation from Crude Oil Vapors,
959 *Environ. Sci. Technol.*, 47(21), 12566–12574, doi:10.1021/es402265y, 2013.

960 Li, R., Palm, B. B., Ortega, A. M., Hu, W., Peng, Z., Day, D. A., Knote, C., Brune, W. H., de Gouw, J. and
961 Jimenez, J. L.: Modeling the radical chemistry in an Oxidation Flow Reactor (OFR): radical formation and
962 recycling, sensitivities, and OH exposure estimation equation, *J. Phys. Chem. A*, 119(19), 4418–4432,
963 doi:10.1021/jp509534k, 2015.

964 Liu, P. F., Abdelmalki, N., Hung, H.-M., Wang, Y., Brune, W. H. and Martin, S. T.: Ultraviolet and visible
965 complex refractive indices of secondary organic material produced by photooxidation of the aromatic
966 compounds toluene and m-Xylene, *Atmos. Chem. Phys.*, 15(3), 1435–1446, doi:10.5194/acp-15-1435-
967 2015, 2015.

968 Liu, P., Zhang, Y. and Martin, S. T.: Complex refractive indices of thin films of secondary organic materials
969 by spectroscopic ellipsometry from 220 to 1200 nm, *Environ. Sci. Technol.*, 47, 13594–13601,
970 doi:10.1021/es403411e, 2013.

971 Mao, J., Ren, X., Brune, W. H., Olson, J. R., Crawford, J. H., Fried, a., Huey, L. G., Cohen, R. C., Heikes, B.,
972 Singh, H. B., Blake, D. R., Sachse, G. W., Diskin, G. S., Hall, S. R. and Shetter, R. E.: Airborne measurement
973 of OH reactivity during INTEX-B, *Atmos. Chem. Phys.*, 9(1), 163–173, doi:10.5194/acp-9-163-2009, 2009.

974 Massoli, P., Lambe, A. T., Ahern, A. T., Williams, L. R., Ehn, M., Mikkilä, J., Canagaratna, M. R., Brune, W.
975 H., Onasch, T. B., Jayne, J. T., Petäjä, T., Kulmala, M., Laaksonen, A., Kolb, C. E., Davidovits, P. and Worsnop,
976 D. R.: Relationship between aerosol oxidation level and hygroscopic properties of laboratory generated
977 secondary organic aerosol (SOA) particles, *Geophys. Res. Lett.*, 37(24), L24801,
978 doi:10.1029/2010GL045258, 2010.

979 Matsunaga, A. and Ziemann, P. J.: Gas-Wall Partitioning of Organic Compounds in a Teflon Film Chamber
980 and Potential Effects on Reaction Product and Aerosol Yield Measurements, *Aerosol Sci. Technol.*, 44(10),
981 881–892, doi:10.1080/02786826.2010.501044, 2010.

982 Messaadia, L., El Dib, G., Ferhati, A. and Chakir, A.: UV–visible spectra and gas-phase rate coefficients
983 for the reaction of 2,3-pentanedione and 2,4-pentanedione with OH radicals, *Chem. Phys. Lett.*, 626,

- 984 73–79, doi:10.1016/j.cplett.2015.02.032, 2015.
- 985 Monks, P. S.: Gas-phase radical chemistry in the troposphere, *Chem. Soc. Rev.*, 34, 376–395,
986 doi:10.1039/b307982c, 2005.
- 987 Nakashima, N.: Laser photolysis of benzene. V. Formation of hot benzene, *J. Chem. Phys.*, 77(12), 6040,
988 doi:10.1063/1.443847, 1982.
- 989 Nakashima, N. and Yoshihara, K.: Laser flash photolysis of benzene. VIII. Formation of hot benzene from
990 the S₂ state and its collisional deactivation, *J. Chem. Phys.*, 79(6), 2727–2735,
991 doi:10.1063/1.446176, 1983.
- 992 Nguyen, T. B., Crounse, J. D., Schwantes, R. H., Teng, a. P., Bates, K. H., Zhang, X., St. Clair, J. M., Brune,
993 W. H., Tyndall, G. S., Keutsch, F. N., Seinfeld, J. H. and Wennberg, P. O.: Overview of the Focused Isoprene
994 eXperiment at the California Institute of Technology (FIXCIT): mechanistic chamber studies on the
995 oxidation of biogenic compounds, *Atmos. Chem. Phys.*, 14(24), 13531–13549, doi:10.5194/acp-14-
996 13531-2014, 2014.
- 997 O’Sullivan, D. W., Neale, P. J., Coffin, R. B., Boyd, T. J. and Osburn, C. L.: Photochemical production of
998 hydrogen peroxide and methylhydroperoxide in coastal waters, *Mar. Chem.*, 97(1-2), 14–33,
999 doi:10.1016/j.marchem.2005.04.003, 2005.
- 1000 Odum, J. R., Hoffmann, T., Bowman, F., Collins, D., Flagan Richard, C. and Seinfeld John, H.: Gas particle
1001 partitioning and secondary organic aerosol yields, *Environ. Sci. Technol.*, 30(8), 2580–2585,
1002 doi:10.1021/es950943+, 1996.
- 1003 Ono, R., Nakagawa, Y., Tokumitsu, Y., Matsumoto, H. and Oda, T.: Effect of humidity on the production
1004 of ozone and other radicals by low-pressure mercury lamps, *J. Photochem. Photobiol. A Chem.*, 274, 13–
1005 19, doi:10.1016/j.jphotochem.2013.09.012, 2014.
- 1006 Ortega, A. M., Day, D. A., Cubison, M. J., Brune, W. H., Bon, D., de Gouw, J. A. and Jimenez, J. L.: Secondary
1007 organic aerosol formation and primary organic aerosol oxidation from biomass-burning smoke in a flow
1008 reactor during FLAME-3, *Atmos. Chem. Phys.*, 13(22), 11551–11571, doi:10.5194/acp-13-11551-2013,
1009 2013.
- 1010 Ortega, A. M., Hayes, P. L., Peng, Z., Palm, B. B., Hu, W., Day, D. A., Li, R., Cubison, M. J., Brune, W. H.,
1011 Graus, M., Warneke, C., Gilman, J. B., Kuster, W. C., de Gouw, J. A. and Jimenez, J. L.: Real-time
1012 measurements of secondary organic aerosol formation and aging from ambient air in an oxidation flow
1013 reactor in the Los Angeles area, *Atmos. Chem. Phys. Discuss.*, 15(15), 21907–21958, doi:10.5194/acpd-
1014 15-21907-2015, 2015.
- 1015 Osburn, C. L., Retamal, L. and Vincent, W. F.: Photoreactivity of chromophoric dissolved organic matter
1016 transported by the Mackenzie River to the Beaufort Sea, *Mar. Chem.*, 115(1-2), 10–20,
1017 doi:10.1016/j.marchem.2009.05.003, 2009.
- 1018 Palm, B. B., Campuzano-Jost, P., Ortega, A. M., Day, D. A., Kaser, L., Jud, W., Karl, T., Hansel, A., Hunter, J.
1019 F., Cross, E. S., Kroll, J. H., Peng, Z., Brune, W. H. and Jimenez, J. L.: In situ secondary organic aerosol
1020 formation from ambient pine forest air using an oxidation flow reactor, *Atmos. Chem. Phys. Discuss.*,
1021 15(21), 30409–30471, doi:10.5194/acpd-15-30409-2015, 2015.
- 1022 Peng, Z., Day, D. A., Stark, H., Li, R., Lee-Taylor, J., Palm, B. B., Brune, W. H. and Jimenez, J. L.: HO_x radical
1023 chemistry in oxidation flow reactors with low-pressure mercury lamps systematically examined by
1024 modeling, *Atmos. Meas. Tech.*, 8(11), 4863–4890, doi:10.5194/amt-8-4863-2015, 2015.
- 1025 Phillips, S. M. and Smith, G. D.: Light Absorption by Charge Transfer Complexes in Brown Carbon Aerosols,
1026 *Environ. Sci. Technol. Lett.*, 1(10), 382–386, doi:10.1021/ez500263j, 2014.
- 1027 Phillips, S. M. and Smith, G. D.: Further Evidence for Charge Transfer Complexes in Brown Carbon
1028 Aerosols from Excitation–Emission Matrix Fluorescence Spectroscopy, *J. Phys. Chem. A*, 119(19), 4545–
1029 4551, doi:10.1021/jp510709e, 2015.
- 1030 Pitts, J. N. and Finlayson, B. J.: Mechanismen der photochemischen Luftverschmutzung, *Angew. Chemie*,
1031 87(1), 18–33, doi:10.1002/ange.19750870103, 1975.
- 1032 Platt, S. M., El Haddad, I., Zardini, a. a., Clairotte, M., Astorga, C., Wolf, R., Slowik, J. G., Temime-Roussel,
1033 B., Marchand, N., Ježek, I., Drinovec, L., Močnik, G., Möhler, O., Richter, R., Barmet, P., Bianchi, F.,

1034 Baltensperger, U. and Prévôt, a. S. H.: Secondary organic aerosol formation from gasoline vehicle
1035 emissions in a new mobile environmental reaction chamber, *Atmos. Chem. Phys.*, 13(18), 9141–9158,
1036 doi:10.5194/acp-13-9141-2013, 2013.

1037 Presto, A. A., Huff Hartz, K. E. and Donahue, N. M.: Secondary Organic Aerosol Production from Terpene
1038 Ozonolysis. 1. Effect of UV Radiation, *Environ. Sci. Technol.*, 39(18), 7036–7045, doi:10.1021/es050174m,
1039 2005.

1040 Pretsch, E., Bühlmann, P. and Badertscher, M.: *Structure Determination of Organic Compounds*, Springer
1041 Berlin Heidelberg, Berlin, Heidelberg., 2009.

1042 Renlund, A. M. and Trott, W. M.: ArF Laser-induced decomposition of simple energetic molecules, *Chem.*
1043 *Phys. Lett.*, 107(6), 555–560, doi:10.1016/S0009-2614(84)85155-6, 1984.

1044 Roberts, J. M. and Fajer, R. W.: UV absorption cross sections of organic nitrates of potential atmospheric
1045 importance and estimation of atmospheric lifetimes, *Environ. Sci. Technol.*, 23(8), 945–951, 1989.

1046 Romonosky, D. E., Ali, N. N., Saiduddin, M. N., Wu, M., Lee, H. J. (Julie), Aiona, P. K. and Nizkorodov, S.
1047 A.: Effective absorption cross sections and photolysis rates of anthropogenic and biogenic secondary
1048 organic aerosols, *Atmos. Environ.*, 130, 172–179, doi:10.1016/j.atmosenv.2015.10.019, 2016.

1049 Romonosky, D. E., Laskin, A., Laskin, J. and Nizkorodov, S. A.: High-Resolution Mass Spectrometry and
1050 Molecular Characterization of Aqueous Photochemistry Products of Common Types of Secondary
1051 Organic Aerosols, *J. Phys. Chem. A*, 119(11), 2594–2606, doi:10.1021/jp509476r, 2015.

1052 Sander, S. P., Friedl, R. R., Barker, J. R., Golden, D. M., Kurylo, M. J., Wine, P. H., Abbatt, J. P. D., Burkholder,
1053 J. B., Kolb, C. E., Moortgat, G. K., Huie, R. E. and Orkin, V. L.: *Chemical Kinetics and Photochemical Data
1054 for Use in Atmospheric Studies Evaluation Number 17.*, 2011.

1055 Saukko, E., Lambe, A. T., Massoli, P., Koop, T., Wright, J. P., Croasdale, D. R., Pedernera, D. A., Onasch, T.
1056 B., Laaksonen, A., Davidovits, P., Worsnop, D. R. and Virtanen, A.: Humidity-dependent phase state of
1057 SOA particles from biogenic and anthropogenic precursors, *Atmos. Chem. Phys.*, 12(16), 7517–7529,
1058 doi:10.5194/acp-12-7517-2012, 2012.

1059 Schmidt, G. a, Kelley, M., Nazarenko, L., Ruedy, R., Russell, G. L., Aleinov, I., Bauer, M., Bauer, S. E., Bhat,
1060 M. K., Bleck, R., Canuto, V., Chen, Y., Cheng, Y., Clune, T. L., Del Genio, A., de Fainchtein, R., Faluvegi, G.,
1061 Hansen, J. E., Healy, R. J., Kiang, N. Y., Koch, D., Lacis, A. a, LeGrande, A. N., Lerner, J., Lo, K. K., Matthews,
1062 E. E., Menon, S., Miller, R. L., Oinas, V., Oloso, A. O., Perlwitz, J. P., Puma, M. J., Putman, W. M., Rind, D.,
1063 Romanou, A., Sato, M., Shindell, D. T., Sun, S., Syed, R. A., Tausnev, N., Tsigaridis, K., Unger, N.,
1064 Voulgarakis, A., Yao, M.-S. and Zhang, J.: Configuration and assessment of the GISS ModelE2
1065 contributions to the CMIP5 archive, *J. Adv. Model. Earth Syst.*, 6(1), 141–184,
1066 doi:10.1002/2013MS000265, 2014.

1067 Seakins, P. W.: A brief review of the use of environmental chambers for gas phase studies of kinetics,
1068 chemical mechanisms and characterisation of field instruments, *EPJ Web Conf.*, 9, 143–163,
1069 doi:10.1051/epjconf/201009012, 2010.

1070 Sharpless, C. M. and Blough, N. V.: The importance of charge-transfer interactions in determining
1071 chromophoric dissolved organic matter (CDOM) optical and photochemical properties, *Environ. Sci.*
1072 *Process. Impacts*, 16(4), 654, doi:10.1039/c3em00573a, 2014.

1073 da Silva, G. and Bozzelli, J. W.: Role of the α -hydroxyethylperoxy radical in the reactions of acetaldehyde
1074 and vinyl alcohol with HO₂, *Chem. Phys. Lett.*, 483(1-3), 25–29, doi:10.1016/j.cplett.2009.10.045, 2009.

1075 Smith, J. D., Kroll, J. H., Cappa, C. D., Che, D. L., Liu, C. L., Ahmed, M., Leone, S. R., Worsnop, D. R. and
1076 Wilson, K. R.: The heterogeneous reaction of hydroxyl radicals with sub-micron squalane particles: a
1077 model system for understanding the oxidative aging of ambient aerosols, *Atmos. Chem. Phys.*, 9(9),
1078 3209–3222, doi:10.5194/acp-9-3209-2009, 2009.

1079 Strollo, C. M. and Ziemann, P. J.: Products and mechanism of secondary organic aerosol formation from
1080 the reaction of 3-methylfuran with OH radicals in the presence of NO_x, *Atmos. Environ.*, 77, 534–543,
1081 doi:10.1016/j.atmosenv.2013.05.033, 2013.

1082 Tkacik, D. S., Lambe, A. T., Jathar, S., Li, X., Presto, A. A., Zhao, Y., Blake, D., Meinardi, S., Jayne, J. T.,
1083 Croteau, P. L. and Robinson, A. L.: Secondary Organic Aerosol Formation from in-Use Motor Vehicle
1084 Emissions Using a Potential Aerosol Mass Reactor, *Environ. Sci. Technol.*, 48(19), 11235–11242,

1085 doi:10.1021/es502239v, 2014.

1086 Tsang, W.: Chemical kinetic data base for combustion chemistry part V. Propene, *J. Phys. Chem. Ref. data*,
1087 20(2), 221–274, doi:10.1063/1.555880, 1991.

1088 Turro, N. J., Ramamurthy, V. and Scaiano, J. C.: *Principles of Molecular Photochemistry: An Introduction*,
1089 University Science Books, Sausalito, CA, USA. [online] Available from:
1090 <http://www.uscibooks.com/turro2.htm>, 2009.

1091 Updyke, K. M., Nguyen, T. B. and Nizkorodov, S. a.: Formation of brown carbon via reactions of ammonia
1092 with secondary organic aerosols from biogenic and anthropogenic precursors, *Atmos. Environ.*, 63, 22–
1093 31, doi:10.1016/j.atmosenv.2012.09.012, 2012.

1094 Wang, B., Lambe, A. T., Massoli, P., Onasch, T. B., Davidovits, P., Worsnop, D. R. and Knopf, D. a.: The
1095 deposition ice nucleation and immersion freezing potential of amorphous secondary organic aerosol:
1096 Pathways for ice and mixed-phase cloud formation, *J. Geophys. Res.*, 117(D16), D16209,
1097 doi:10.1029/2012JD018063, 2012.

1098 Wang, J., Doussin, J. F., Perrier, S., Perraudin, E., Katrib, Y., Pangui, E. and Picquet-Varrault, B.: Design of
1099 a new multi-phase experimental simulation chamber for atmospheric photochemistry, aerosol and cloud
1100 chemistry research, *Atmos. Meas. Tech.*, 4(11), 2465–2494, doi:10.5194/amt-4-2465-2011, 2011.

1101 Warneke, C., Roberts, J. M., Veres, P., Gilman, J., Kuster, W. C., Burling, I., Yokelson, R. and de Gouw, J.
1102 a.: VOC identification and inter-comparison from laboratory biomass burning using PTR-MS and PIT-MS,
1103 *Int. J. Mass Spectrom.*, 303(1), 6–14, doi:10.1016/j.ijms.2010.12.002, 2011.

1104 Wong, J. P. S., Zhou, S. and Abbatt, J. P. D.: Changes in Secondary Organic Aerosol Composition and Mass
1105 due to Photolysis: Relative Humidity Dependence, *J. Phys. Chem. A*, 119(19), 4309–4316,
1106 doi:10.1021/jp506898c, 2015.

1107 Zhang, X., Cappa, C. D., Jathar, S. H., McVay, R. C., Ensberg, J. J., Kleeman, M. J. and Seinfeld, J. H.:
1108 Influence of vapor wall loss in laboratory chambers on yields of secondary organic aerosol., *Proc. Natl.*
1109 *Acad. Sci. U. S. A.*, 111(16), 5802–7, doi:10.1073/pnas.1404727111, 2014.

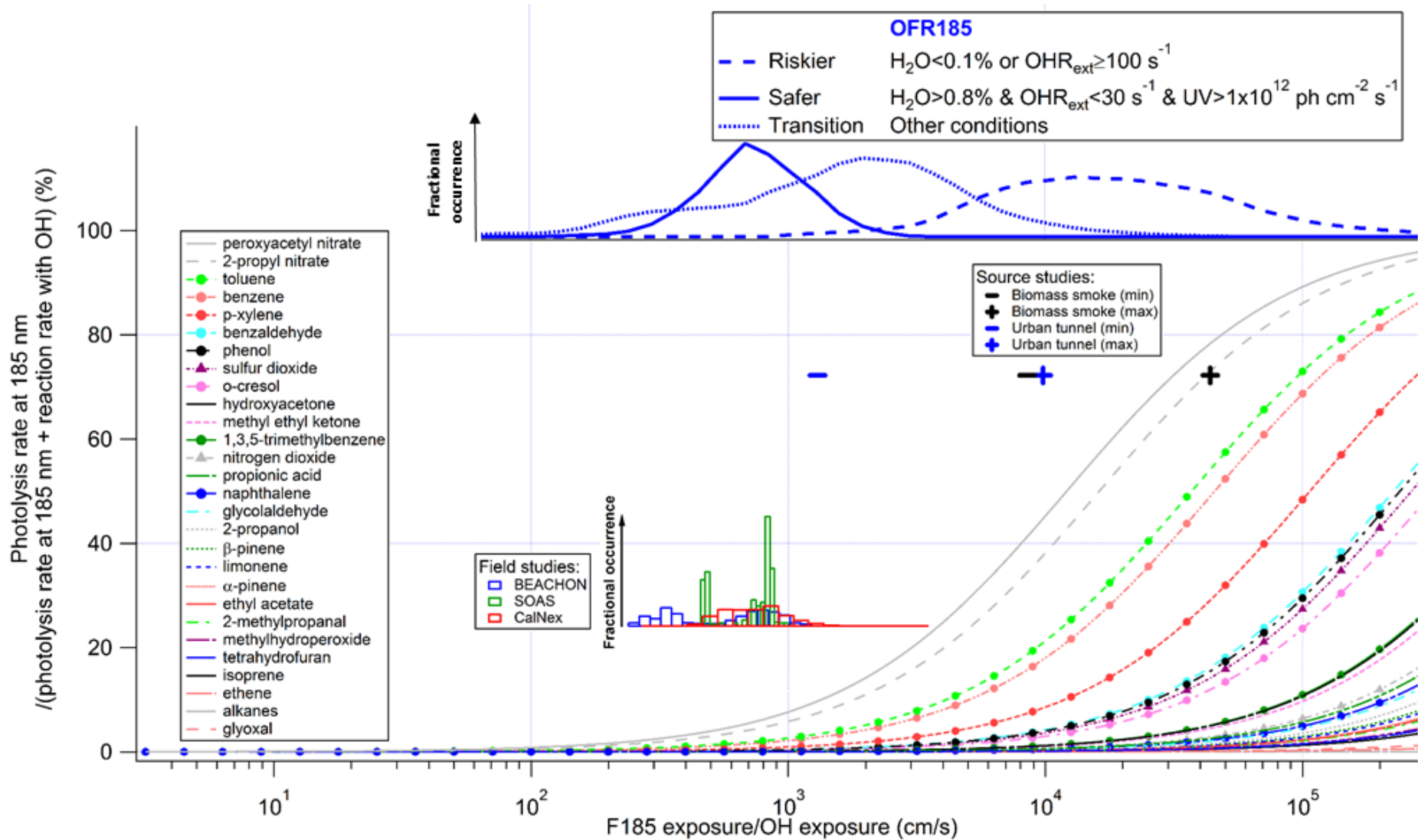
1110 Zhang, Y., Xie, H. and Chen, G.: Factors Affecting the Efficiency of Carbon Monoxide Photoproduction in
1111 the St. Lawrence Estuarine System (Canada), *Environ. Sci. Technol.*, 40(24), 7771–7777,
1112 doi:10.1021/es0615268, 2006.

1113 Ziemann, P. and Atkinson, R.: Kinetics, products, and mechanisms of secondary organic aerosol
1114 formation, *Chem. Soc. Rev.*, 41(19), 6582, doi:10.1039/c2cs35122f, 2012.

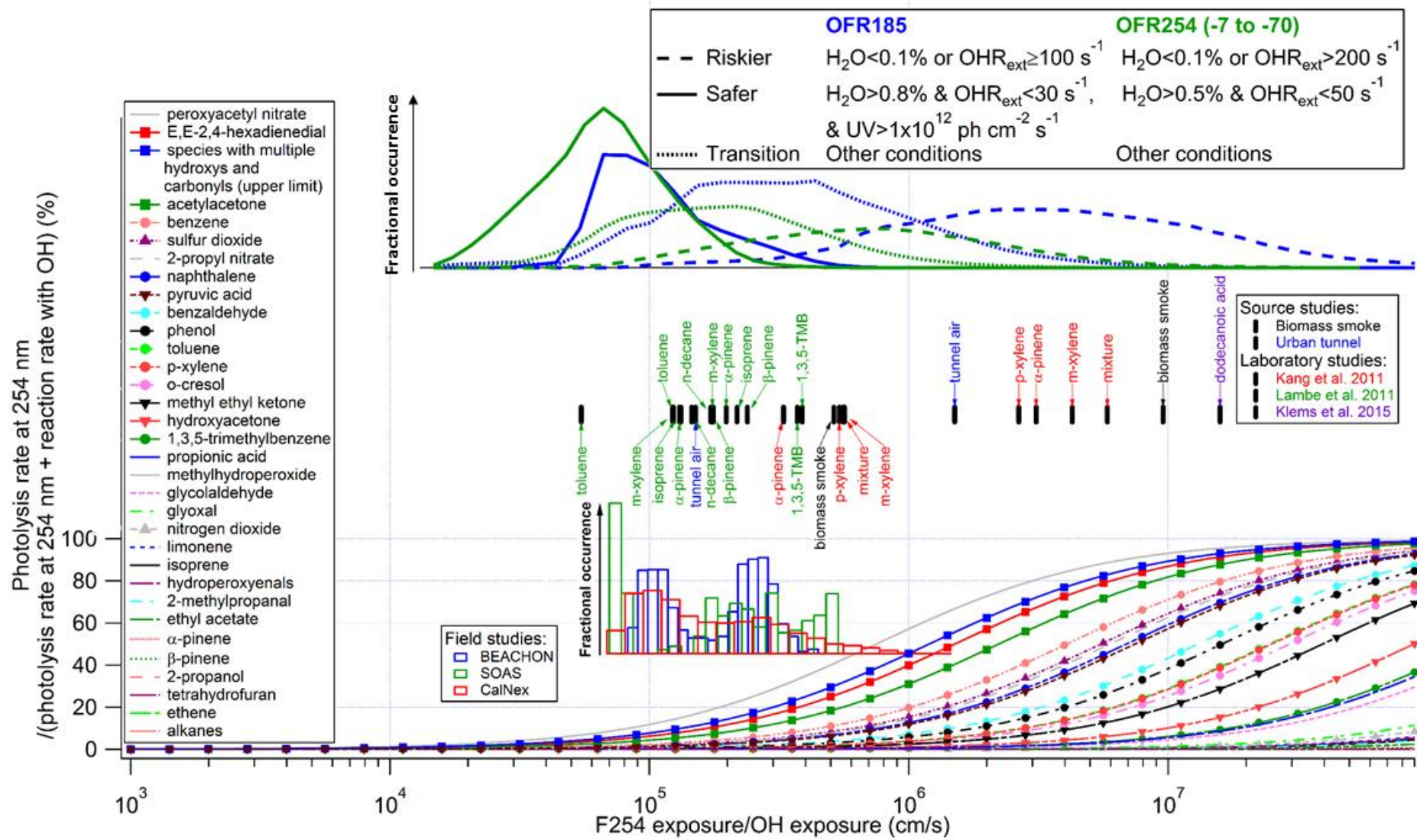
1115

1116

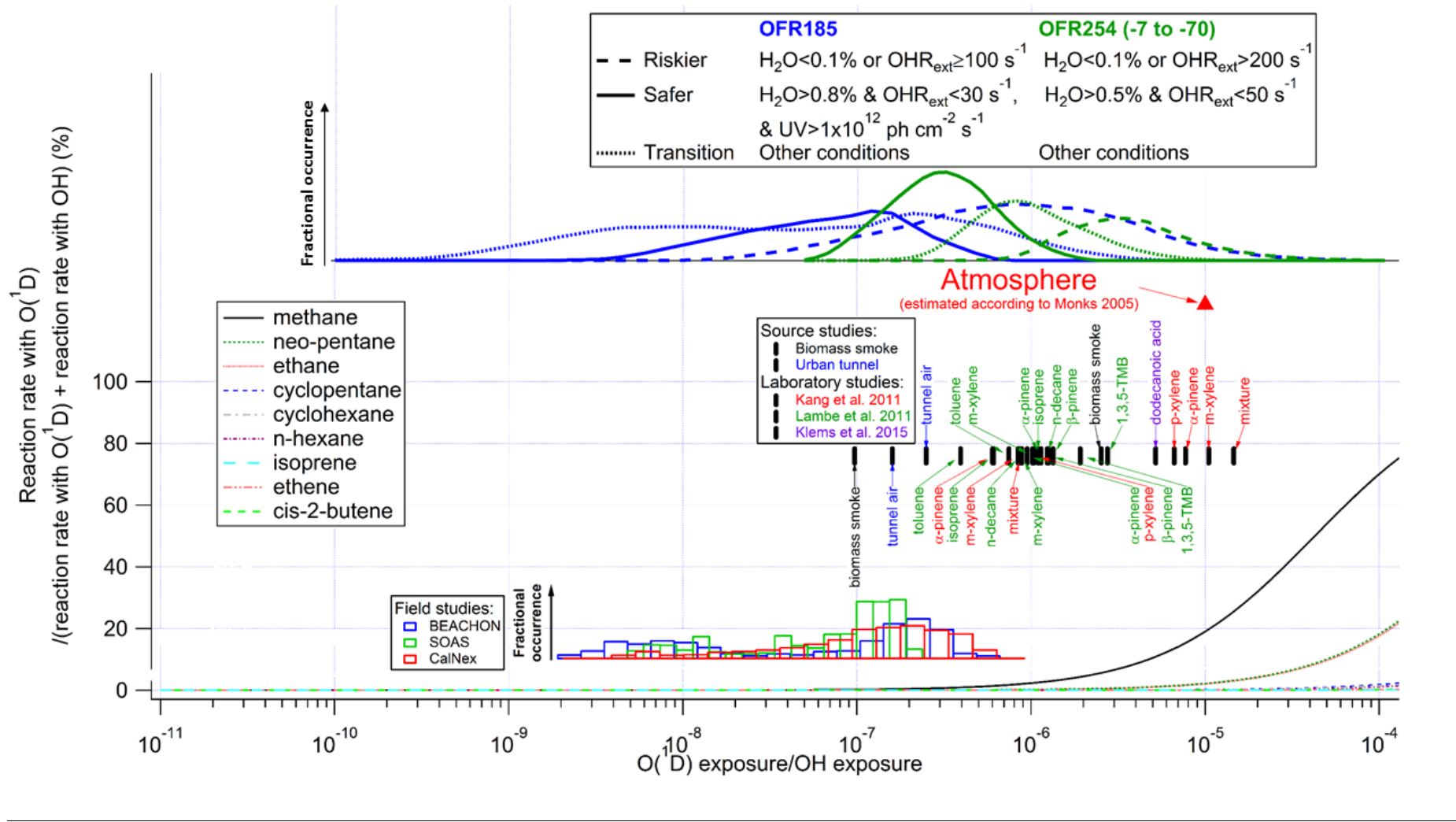
1117



1119 **Figure 1.** Fractional importance of the photolysis rate at 185 nm of several species of interest vs. the reaction rate with OH, as a function of the ratio of exposure to 185 nm
1120 photons (F185) and OH. F185 exposure (in photons cm^{-2}) is the product of 185 nm photon flux (in photons $\text{cm}^{-2} \text{s}^{-1}$) and time (in s). F185 exposure / OH exposure is thus in cm
1121 s^{-1} . The modeled frequency distributions of ratios of 185 nm photon exposure to OH exposure under riskier, safer, and transition conditions for OFR185 are also shown. The
1122 curves of aromatics and inorganic gases are highlighted by solid dots and upward triangles, respectively. The lower inset shows histograms of model-estimated F185/OH
1123 exposures for three field studies where OFR185 was used to process ambient air. Their ordinate is the fractional occurrence of a given condition ($X_{\text{exp}}/\text{OH}_{\text{exp}}$). All histograms are
1124 normalized to be of identical total area (i.e., total probability of 1). The upper inset (black and blue markers) shows similar information for source studies of biomass smoke
1125 (FLAME-3; Ortega et al., 2013) and an urban tunnel (Tkacik et al., 2014). All curves, markers, and histograms in this figure share the same abscissa.

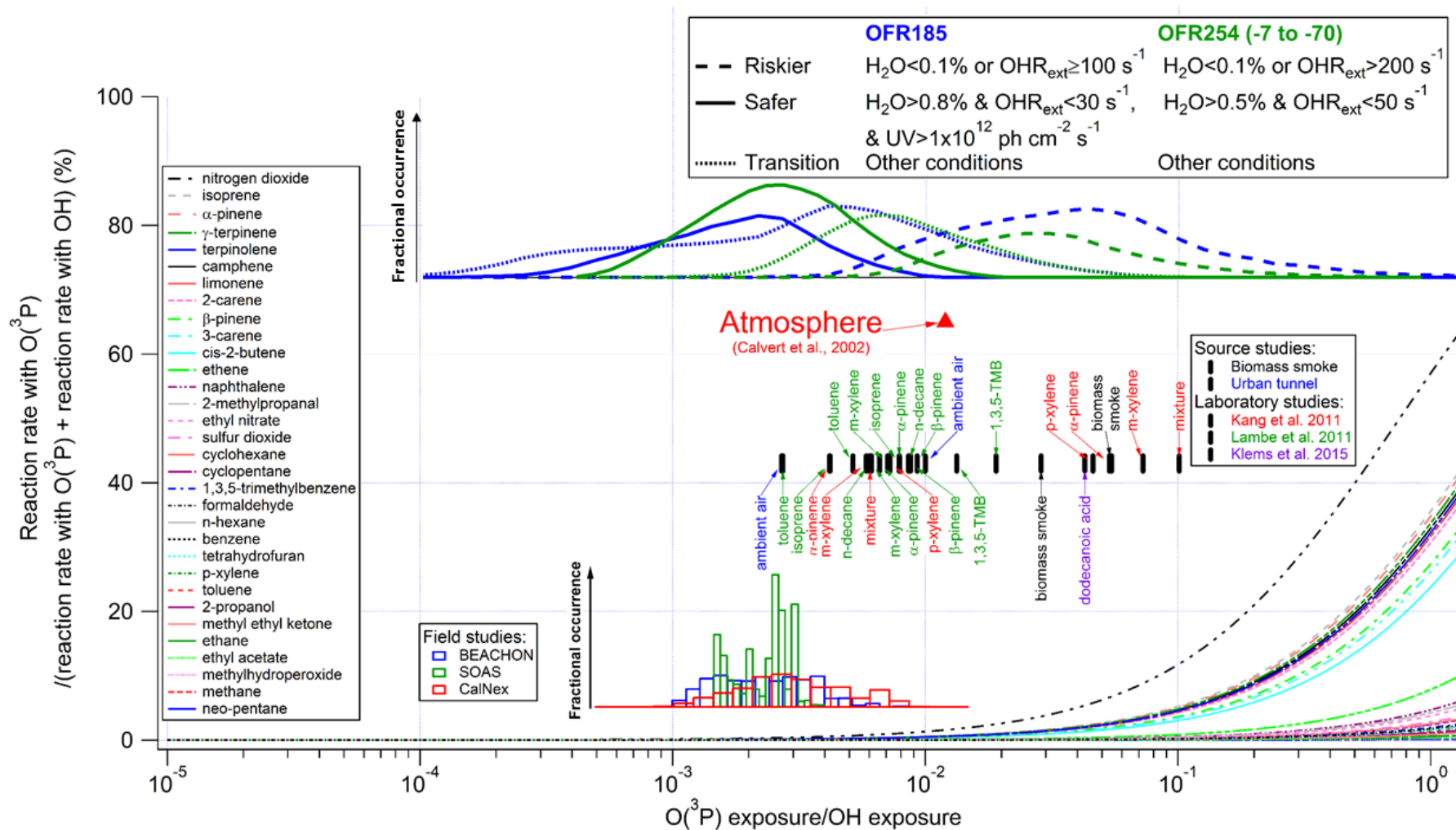


1127 **Figure 2.** Same format as Fig. 1, but for the fractional importance of the photolysis rate at 254 nm vs. the reaction rate with OH as a function of the ratio of exposure to 254 nm
1128 (F254) and OH. The modeled frequency distributions of ratios of 254 nm photon exposure to OH exposure under riskier, safer, and transition conditions for OFR185 and OFR254
1129 (-7 to -70) are also shown. The curves of saturated carbonyl compounds and possible highly absorbing oxidation intermediates are highlighted by downward triangles and
1130 squares, respectively. The insets show histograms of model-estimated F254/OH exposures for three field studies where OFR185 was used to process ambient air. In addition to
1131 source studies of biomass smoke (FLAME-3) and urban tunnel (Tkacik et al., 2014), F254 exposure/OH exposure ratios in two laboratory studies (Kang et al., 2011; Lambe et al.,
1132 2011b) are shown in the upper inset. Colored tags indicate species used in the laboratory experiments. The lower and upper limits of F254 exposure/OH exposure ratios in the
1133 experiments with a certain source in a certain study are denoted by tags below and above the markers, respectively.



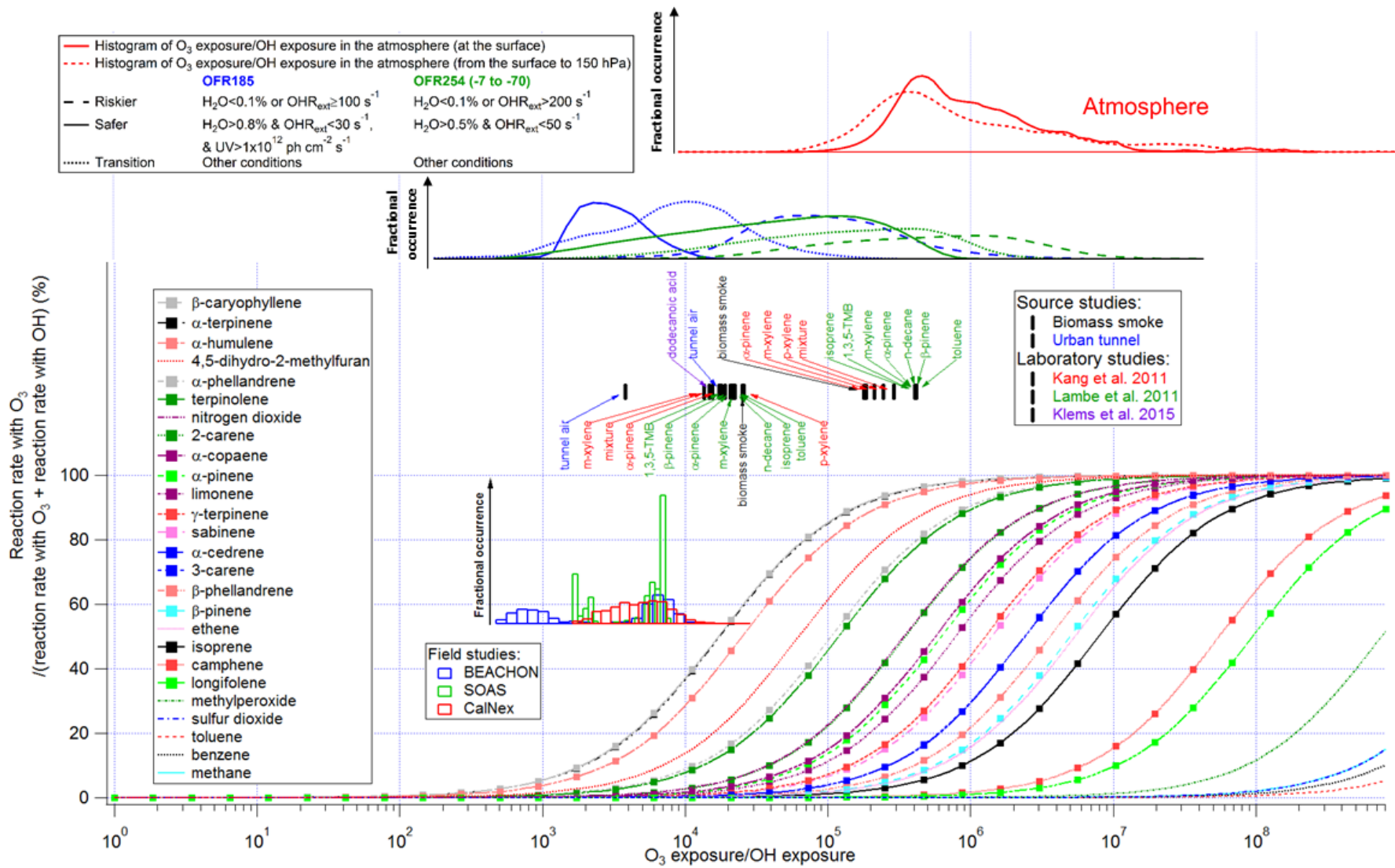
1134
1135
1136

Figure 3. Same format as Fig. 2, but for the ratio of the reaction rate with $O(^1D)$ vs. OH as a function of the relative exposure to $O(^1D)$ and OH. A typical value of the relative exposure of $O(^1D)$ and OH in the troposphere estimated according to Monks (2005) is also shown.

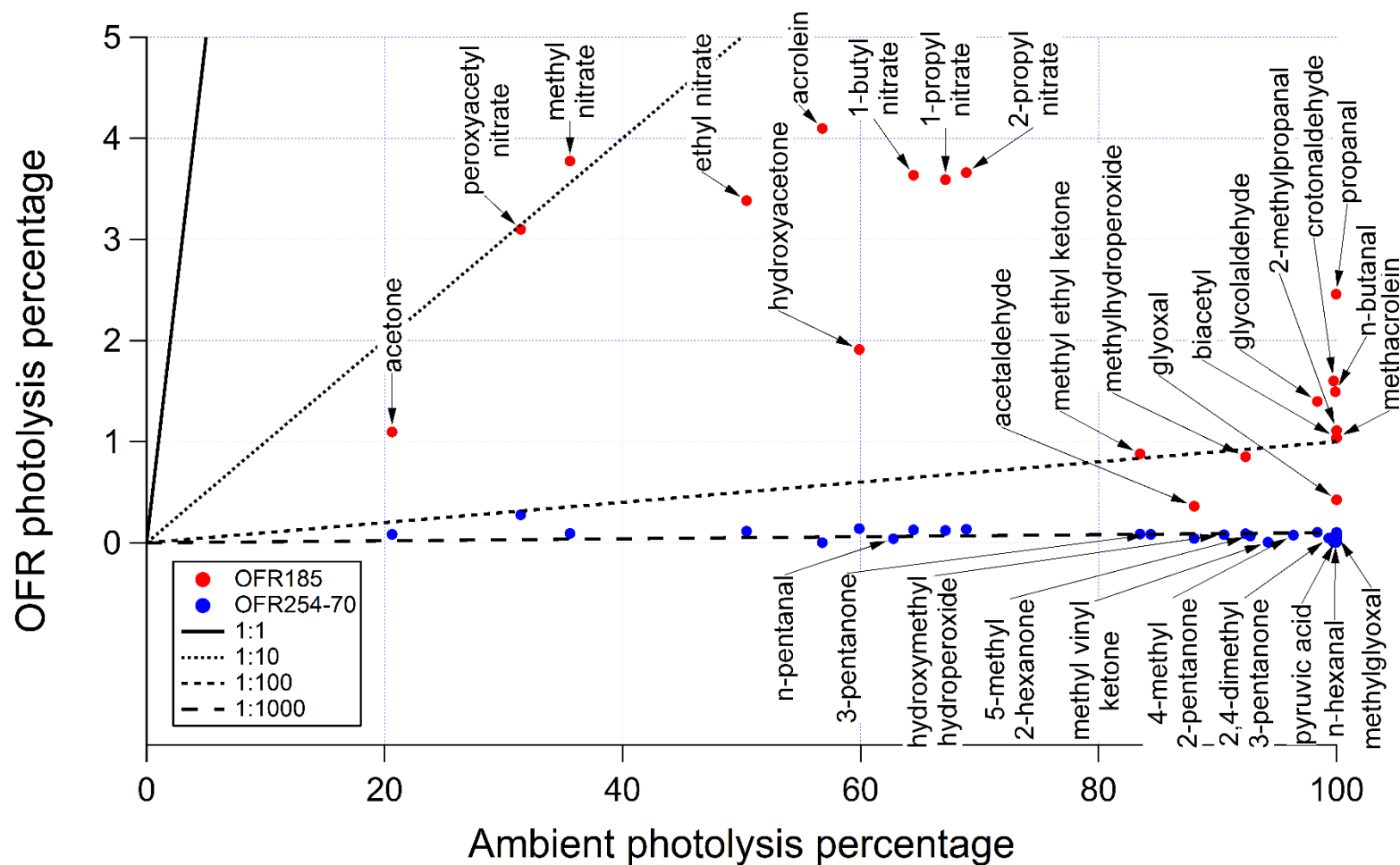


1137
 1138
 1139

Figure 4. Same format as Fig. 3, but for the ratio of the reaction rate with $O(^3P)$ vs. OH as a function of the relative exposure of $O(^3P)$ and OH. A typical value of the relative exposure of $O(^3P)$ and OH in the troposphere from Calvert et al. (2002) is also shown.

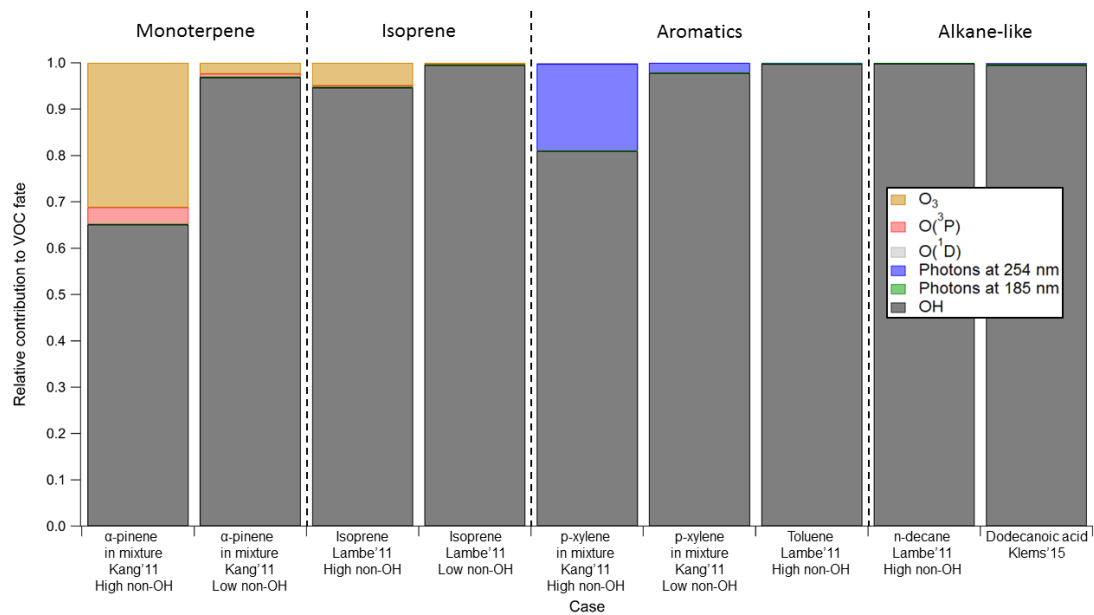


1141 **Figure 5.** Same format as Fig. 2, but for the fractional importance of the reaction rate with O₃ vs. OH as a function of the relative exposure of O₃ and OH. The curves of biogenics
1142 are highlighted by squares. Also shown are modeled distributions of the relative exposure of O₃ and OH at the Earth's surface (solid line) and throughout the column from the
1143 surface to a height with a pressure of 150 hPa (dashed line). The distributions were calculated from the mean daily concentrations of O₃ and OH as simulated by the GISS
1144 ModelE2.

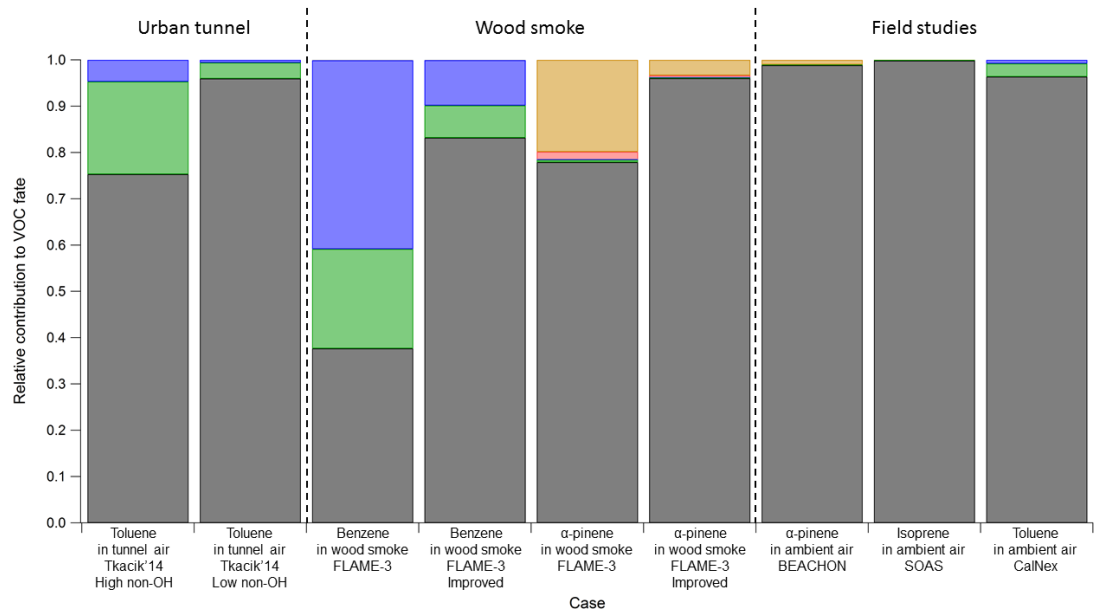


1145
 1146
 1147
 1148
 1149
 1150

Figure 6. Ambient photolysis fractions of secondary species in a week (calculated from photolysis rates reported in Hodzic et al. (2015)) vs. photolysis fractions of those species in OFR185 and OFR254-70 when reaching the same photochemical age (ambient OH concentration of 1.5×10^6 molecules cm^{-3} assumed) under conditions of 70% relative humidity (water vapor mixing ratio of 1.4%) and 25 s^{-1} initial OHR_{ext} . If the points of a certain species for both OFR185 and OFR254-70 are available, the species name is tagged on the OFR185 point (downward arrow), otherwise on the OFR254-70 point (upward arrow). The 1:1, 1:10, 1:100, and 1:1000 lines are also shown for comparison.



1151

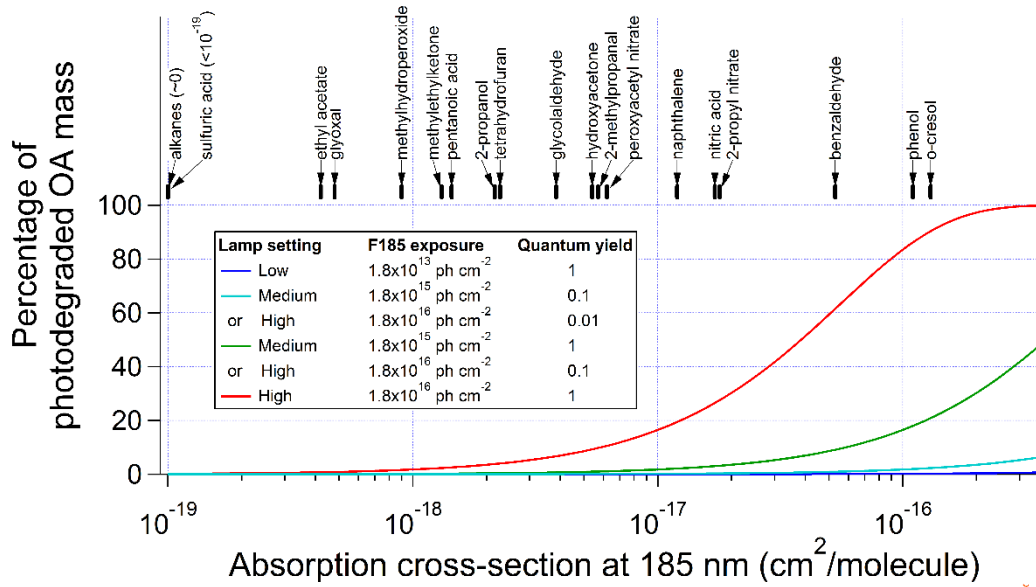


1152

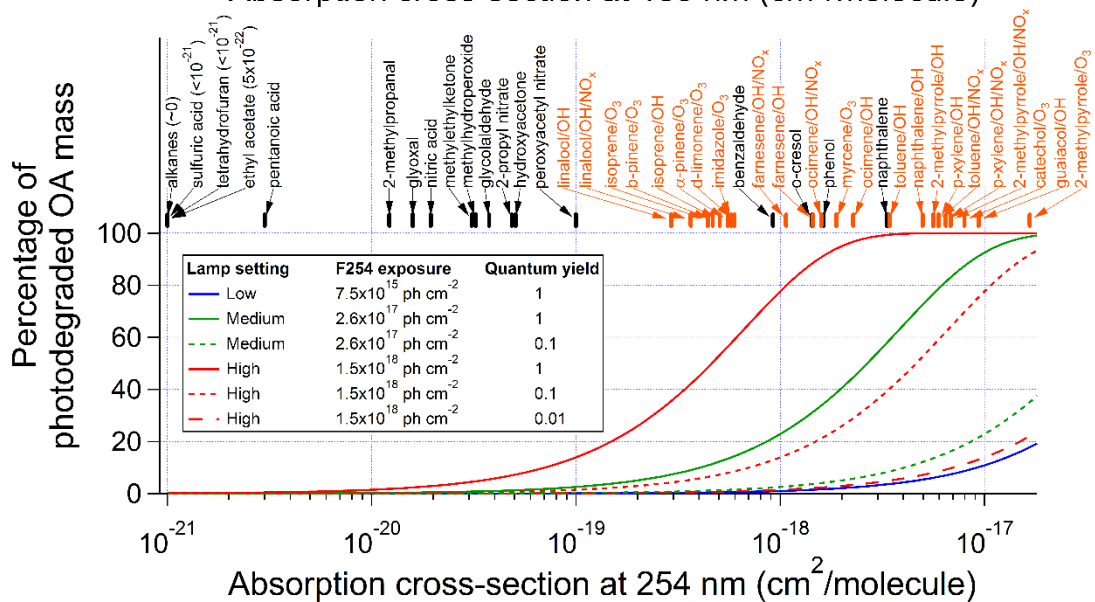
1153

1154

Figure 7. VOC fate in several representative cases of the laboratory, source, and field studies examined in this work. More details on VOC fate in these studies can be found in Table S4.



1155



1156

1157 **Figure 8.** Percentage of SOA photodegradation at (upper panel) 185 and (lower panel) 254 nm at different
 1158 UV levels as a function of absorption cross-section under the assumptions of quantum yields of 1, 0.1,
 1159 and 0.01. Absorption cross-sections of some SOA component surrogates (black tag) and SOA samples
 1160 (orange tag; calculated from data in Lambe et al. (2013) and Romonosky et al. (2015a)) are also shown.

1161 **Table 1.** Code of the labels of typical cases. A case label is composed of three characters denoting the
 1162 water mixing ratio, the photon flux, and the external OH reactivity, respectively.

	Water mixing ratio	Photon flux	External OH reactivity
	L=low (0.07%)	L=low (10^{11} photons $\text{cm}^{-2} \text{s}^{-1}$ at 185 nm; 4.17×10^{13} photons $\text{cm}^{-2} \text{s}^{-1}$ at 254 nm)	0
Options	M=medium (1%)	M=medium (10^{13} photons $\text{cm}^{-2} \text{s}^{-1}$ at 185 nm; 1.45×10^{15} photons $\text{cm}^{-2} \text{s}^{-1}$ at 254 nm)	L=low (10 s^{-1}) typically for remote or clean urban air
	H=high (2.3%)	H=high (10^{14} photons $\text{cm}^{-2} \text{s}^{-1}$ at 185 nm; 8.51×10^{15} photons $\text{cm}^{-2} \text{s}^{-1}$ at 254 nm)	H=high (100 s^{-1}) typically for polluted urban air
		"L"=lowest in Li et al. (2015)'s PAM (7.9×10^{11} photons $\text{cm}^{-2} \text{s}^{-1}$ at 185 nm; 2.04×10^{14} photons $\text{cm}^{-2} \text{s}^{-1}$ at 254 nm)	V=very high (1000 s^{-1}) only for laboratory experiments
Example	LH0:	low water mixing ratio, high photon flux, no external OH reactivity	

1163
 1164